



**HAL**  
open science

## Pseudo-first-order reaction of chemically and biologically formed green rusts with HgII and C<sub>15</sub>H<sub>15</sub>N<sub>3</sub>O<sub>2</sub>: effects of pH and stabilizing agents (phosphate, silicate, polyacrylic acid, and bacterial cells)

P-Ph Remy, M. Etique, A. A. Hazotte, A-S Sergent, N. Estrade, C. Cloquet, K. Hanna, F. P. A. Jorand

### ► To cite this version:

P-Ph Remy, M. Etique, A. A. Hazotte, A-S Sergent, N. Estrade, et al.. Pseudo-first-order reaction of chemically and biologically formed green rusts with HgII and C<sub>15</sub>H<sub>15</sub>N<sub>3</sub>O<sub>2</sub>: effects of pH and stabilizing agents (phosphate, silicate, polyacrylic acid, and bacterial cells). *Water Research*, 2015, 70, pp.266-278. 10.1016/j.watres.2014.12.007 . hal-01153424

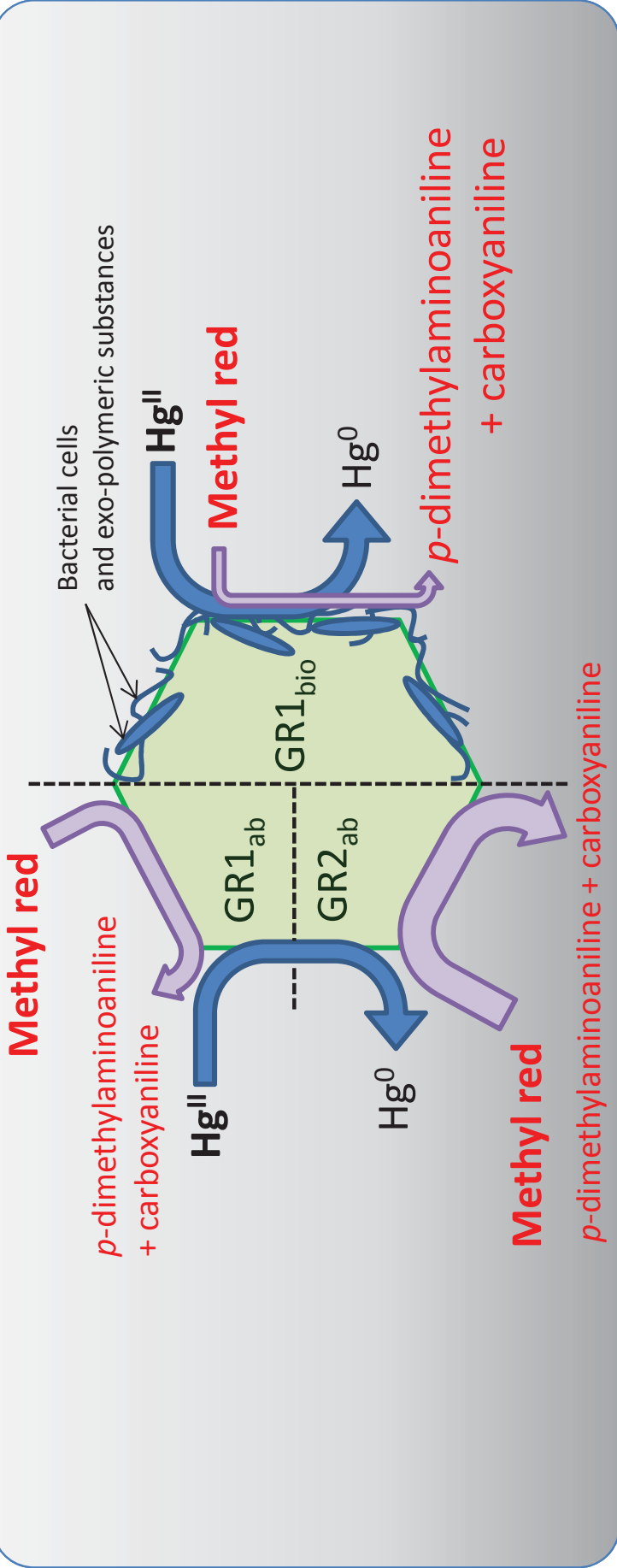
**HAL Id: hal-01153424**

**<https://univ-rennes.hal.science/hal-01153424v1>**

Submitted on 22 Oct 2015

**HAL** is a multi-disciplinary open access archive for the deposit and dissemination of scientific research documents, whether they are published or not. The documents may come from teaching and research institutions in France or abroad, or from public or private research centers.

L'archive ouverte pluridisciplinaire **HAL**, est destinée au dépôt et à la diffusion de documents scientifiques de niveau recherche, publiés ou non, émanant des établissements d'enseignement et de recherche français ou étrangers, des laboratoires publics ou privés.



1 **Pseudo-first-order reaction of chemically and biologically formed green**  
2 **rusts with Hg<sup>II</sup> and C<sub>15</sub>H<sub>15</sub>N<sub>3</sub>O<sub>2</sub>: effects of pH and stabilizing agents**  
3 **(phosphate, silicate, polyacrylic acid, and bacterial cells)**

4 P.-Ph. Remy<sup>1,2</sup>, M. Etique<sup>1,2</sup>, A.A. Hazotte<sup>1,2,§</sup>, A.-S. Sergent<sup>1,2</sup>, N. Estrade<sup>3,4#</sup>, C. Cloquet<sup>3,4</sup>,  
5 K. Hanna<sup>5,6</sup>, and F.P.A. Jorand<sup>1,2\*</sup>

6  
7 <sup>1</sup>Université de Lorraine, LCPME, UMR 7564, Institut Jean Barriol, Villers-lès-Nancy, F-  
8 54601, France

9 <sup>2</sup>CNRS, LCPME, UMR 7564, Institut Jean Barriol, Villers-lès-Nancy, F-54601, France

10 <sup>3</sup>CNRS, CRPG, UMR 7358, BP 20, Vandœuvre-lès-Nancy, F-54501, France

11 <sup>4</sup>Université de Lorraine, CRPG, UMR 7358, BP 20, Vandœuvre-lès-Nancy, F-54501, France

12 <sup>5</sup>ENSCR, CNRS, UMR 6226, CS 50837, Rennes Cedex 7, F-35708, France

13 <sup>6</sup>Université européenne de Bretagne, Rennes, F-35000, France

14 <sup>§</sup>Present address: LUNAM University, Subatech-LPGN, UMR 6457 & 6112, BP 92208, F-  
15 44322 Nantes Cedex 3, France

16 <sup>#</sup>Present address: Pacific Centre for Isotopic and Geochemical Research, EOAS, The  
17 University of British Columbia, 2207 Main Mall, Vancouver, British Columbia, V6T 1Z4,  
18 Canada.

19  
20 \*Corresponding author: frederic.jorand@univ-lorraine.fr; +33 (0)383 685 248

21 **Keywords:** Reductive transformation, layered double hydroxides, cationic mercury, methyl  
22 red, biogenic green rust, surface area concentration

23

24 **Abstract**

25       The kinetics of Hg<sup>II</sup> and methyl red (MR) reduction by hydroxycarbonate green rust  
26 (GR1) and by hydroxysulfate green rust (GR2) were studied in the presence of naturally  
27 occurring organic and inorganic ligands (phosphate, polyacrylic acid, bacterial cells, silicate).  
28 The reducing ability of biogenic hydroxycarbonate green rust (GR1<sub>bio</sub>), obtained after  
29 microbial reduction of lepidocrocite by *Shewanella putrefaciens*, was also investigated and  
30 compared to those of chemically synthesized GR1 and GR2 (GR1<sub>ab</sub> and GR2<sub>ab</sub>). Pseudo first-  
31 order rate constants ( $k_{\text{obs}}$ ) of Hg<sup>II</sup> reduction (at pH 7, 8.2, and 9.5) and MR reduction (at pH 7)  
32 were determined and were normalized to the structural Fe<sup>II</sup> content of GRs ( $k_{\text{FeII}}$ ) and to the  
33 estimated concentration of surface Fe<sup>II</sup> sites ( $k_{\text{S}}$ ). The  $k_{\text{S}}$  values ranged from 0.3 L mmol<sup>-1</sup>  
34 min<sup>-1</sup> to 43 L mmol<sup>-1</sup> min<sup>-1</sup> for the Hg reduction, and from 0.007 L mmol<sup>-1</sup> min<sup>-1</sup> to  
35 3.4 L mmol<sup>-1</sup> min<sup>-1</sup> for the MR reduction. No significant discrepancy between GR<sub>ab</sub> and GR<sub>bio</sub>  
36 was observed in term of reactivity. However, the reduction kinetics of MR was generally  
37 slower than the Hg<sup>II</sup> reduction kinetics for all tested GRs. While a slight difference in Hg<sup>II</sup>  
38 reduction rate was noted whatever the pH values (7.0, 8.2, or 9.5), the reduction of MR was  
39 significantly affected in the presence of ligands. A decrease by a factor of 2 – 200, depending  
40 on the type of ligand used, was observed. These data give new insights into the reactivity of  
41 GRs in the presence of co-occurring organic and inorganic ligands, and have major  
42 implications in the characterization of contaminated systems as well as water treatment  
43 processes.

44

## 45 1. Introduction

46 Green rusts (GRs) are mixed ferrous–ferric hydroxides which have a layered structure  
47 characterized by alternating positively charged hydroxide layers  $\{\text{Fe}^{\text{II}}_{(1-x)}\text{Fe}^{\text{III}}_x(\text{OH})_2\}^{x+}$  and  
48 hydrated anionic interlayers  $\{(x/n)\text{A}^{n-} \cdot m\text{H}_2\text{O}\}^{x-}$ . Two types of GRs are distinguished: green  
49 rust 1 (GR1) and green rust 2 (GR2) containing either planar or spherical anions (*e.g.*  $\text{CO}_3^{2-}$ ,  
50  $\text{Cl}^-$ ), and non-planar anions (*e.g.*  $\text{SeO}_4^{2-}$ ,  $\text{SO}_4^{2-}$ ), respectively (Génin *et al.*, 2006). GRs are  
51 present in the environment as corrosion products of Fe-based materials (Refait *et al.*, 2003),  
52 and as minerals (*e.g.* fougèrite) in hydromorphic soils (Génin *et al.*, 1998), in ground water  
53 (Christiansen *et al.*, 2009), or in suspended matter of stratified lakes (Zegeye *et al.*, 2012).  
54 GRs are described as highly reactive compounds, especially in reducing several organic and  
55 inorganic contaminants (Myneni *et al.*, 1997; Erbs *et al.*, 1999; Loyaux-Lawniczak *et al.*,  
56 2000; Hansen *et al.*, 2001; Williams and Scherer, 2001; Lee and Batchelor, 2002; O’Loughlin  
57 *et al.*, 2003; Elsner *et al.*, 2004; O’Loughlin *et al.*, 2004; Mitsunobu *et al.*, 2008; Kone *et al.*,  
58 2009) and their roles in the biogeochemical redox cycling of iron and other elements are of  
59 growing interest to the scientific community (*e.g.* : Carlson *et al.*, 2012; Zegeye *et al.*, 2012).  
60 Although their reactivity has been widely investigated with chemically synthesized GR2  
61 ( $\text{SO}_4^{2-}$ ), the reactivity of GR1, microbially synthesized GR1/GR2, and GR2 in the presence of  
62 cells or polymers has been scarcely reported.

63 GRs can be synthesized at the laboratory scale by a partial oxidation of ferrous salts or  
64 by a coprecipitation of  $\text{Fe}^{\text{II}}$  with  $\text{Fe}^{\text{III}}$  salts in aqueous solution (Schwertmann and Fechter,  
65 1994; Génin *et al.*, 1998; Bocher *et al.*, 2004). They can also be formed by bacterial activities  
66 via a bioreduction of ferrihydrite or lepidocrocite under anoxic conditions (Fredrickson *et al.*,  
67 1998; Ona-Nguema *et al.*, 2002) or by an indirect  $\text{Fe}^{\text{II}}$  oxidation by biogenic nitrite (Etique *et*  
68 *al.*, 2014a). In the natural environment, the formation of GRs is sometimes incorrectly  
69 considered as a biological process, whereas the reduction of  $\text{Fe}^{\text{III}}$  species or the oxidation of

70 Fe<sup>II</sup> species are only due to an enzymatic reaction. The resulting coprecipitation leading to the  
71 formation of GR in the extracellular medium is only based on a chemical process.  
72 Furthermore, no difference in structure and composition between chemically and biologically  
73 formed GRs have been evidenced, except for the size of crystals, which are larger for the  
74 biological GR than for its chemical counterpart (Zegeye *et al.*, 2005), and for the presence of  
75 extracellular-polymeric substances (EPS) and/or bacterial cells surrounding biological GR  
76 crystals (Zegeye *et al.*, 2010; Jorand *et al.*, 2013). These EPS and cells are perceived as  
77 affecting GR reactivity, which might explain the higher stability of the biogenic GR (for  
78 several years in aqueous phase) as compared to the chemical one. However, this phenomenon  
79 remains poorly studied and barely understood. Although recent work has demonstrated that  
80 the extracellular polymers (EPS from activated sludge in waste water treatment) significantly  
81 affect the reactivity of GR1 towards anionic inorganic pollutants (NO<sub>3</sub><sup>-</sup>), probably by “screen  
82 effect” on reactive sites (Zegeye *et al.*, 2014), knowledge on this reactivity with metallic or  
83 organic contaminants is essential to provide greater insight into applied or natural processes in  
84 which GRs are involved (*e.g.* Su and Puls, 2004; Bearcock *et al.*, 2011).

85 For that purpose, the reactivity of a biologically/chemically synthesized  
86 hydroxycarbonate GR1 (GR1<sub>bio</sub>/GR1<sub>ab</sub>), and chemically formed sulfate GR2 (GR2<sub>ab</sub>) towards  
87 Hg<sup>II</sup> and C<sub>15</sub>H<sub>15</sub>N<sub>3</sub>O<sub>2</sub> (methyl red MR) was investigated in presence of various stabilizing  
88 agents. Previous works have already studied the reactivity of GR2<sub>ab</sub> towards Hg<sup>II</sup> and MR  
89 (O’Loughlin *et al.*, 2003; Kone *et al.*, 2009), but to the best of our knowledge, the reactivity  
90 of biogenic GRs towards these two contaminants has not yet been documented. In anoxic  
91 environments, green rust phases are represented by the fougèrite mineral, which is a  
92 hydroxycarbonate green rust (GR1) (Génin *et al.*, 1998; Mills *et al.*, 2012). Therefore, the  
93 most representative iron phase of this fougèrite mineral would be the GR1<sub>bio</sub>. GR2<sub>ab</sub> is known  
94 to be relatively stable as long as common anoxic conditions are preserved at pH ~7 (Ruby *et*

95 *al.*, 2006), while GR1<sub>ab</sub> is perceived as unstable iron hydroxides rapidly turning into a mixture  
96 of magnetite (Fe<sup>II</sup>Fe<sup>III</sup><sub>2</sub>O<sub>4</sub>) and siderite (FeCO<sub>3</sub>) (Taylor *et al.*, 1985; Benali *et al.*, 2001).  
97 However, under strict anoxic conditions and neutral to slightly alkaline pH (7 – 9) (this work),  
98 GR1<sub>ab</sub> can be preserved and stored for several days (Etique *et al.*, 2014b). Nonetheless, many  
99 experiments were performed with GR1<sub>ab</sub> supplemented with PO<sub>4</sub><sup>3-</sup> that prevents any further  
100 undesirable “transformation” (Bocher *et al.*, 2004). Silicate, quartz, organic polymers, and  
101 bacterial cells – compounds which are commonly found in environmental settings or in water  
102 or soil remediation processes – were also described to inhibit/prevent GRs  
103 dissolution/transformation (Zegeye *et al.*, 2010; O’Loughlin *et al.*, 2010; Sergent *et al.*, 2011;  
104 Jorand *et al.*, 2013). Thus, to test the ability of these “stabilizers” to affect the reactivity of  
105 GR1 and GR2, the reduction of Hg<sup>II</sup> and MR was carried out in the presence of phosphates,  
106 silicates, polyacrylic acid (paa), and bacterial cells, at pH values allowing a stability of GRs  
107 (pH > 7). Control experiments were also performed to evaluate the contribution of aqueous  
108 Fe<sup>II</sup> and bacterial cells to the transformation of target compounds. The depletion of mercury  
109 was monitored over time using ICP-AAS. The MR reduction was monitored by UV-Visible  
110 spectrophotometry.

111

## 112 **2. Chemical background**

### 113 **2.1. Mercury and GR**

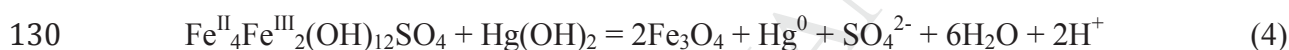
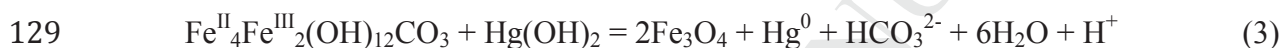
114 Mercury has two main stable oxidation states: Hg<sup>0</sup> and Hg<sup>II</sup>. Elemental Hg<sup>0</sup> is gaseous  
115 under environmental conditions, and under environmentally relevant pH values Hg<sup>II</sup> exists in  
116 pure water in aqueous form as Hg<sup>2+</sup> and mercury dihydroxide (Hg(OH)<sub>2</sub>) (1) with a p*K*<sub>a</sub> value  
117 of 6.09 (Pourbaix, 1963):



119 Thus, the predominant mercury species with pH higher than or equal to 6.09 is Hg(OH)<sub>2</sub>, and  
 120 the reduction half-reaction equation (2) is:



122 The reduction of Hg<sup>II</sup> is effective in the presence of solid Fe<sup>II</sup> but insignificant with aqueous  
 123 Fe<sup>II</sup> (Charlet *et al.*, 2002). The mixed Fe<sup>II</sup>-Fe<sup>III</sup> minerals, such as sulfate GR2, are oxidized by  
 124 Hg<sup>II</sup> to magnetite (O'Loughlin *et al.* 2003). The Fe<sup>II</sup>/Fe<sup>III</sup> ratio of hydroxycarbonate GR1 can  
 125 vary from 1/2 to 2/1 (trébeurdenite and fougèrite, respectively) (Mills *et al.*, 2012), while it is  
 126 equal to 2/1 for sulfate GR2, as far as we know (Refait *et al.*, 2006). The oxidation of GR1  
 127 and GR2 to magnetite by Hg(OH)<sub>2</sub> involves an exchange of 2 electrons and is given by  
 128 equations (3) and (4):



131 Due to the presence of bicarbonate, the oxidation of GR1 leads to a lower production of H<sup>+</sup>  
 132 than that of GR2.

## 133 2.2. Methyl red and GR

134 Methyl red (MR) or 2-(N,N-dimethyl-4-aminophenyl)azobenzenecarboxylic acid  
 135 (C<sub>15</sub>H<sub>15</sub>N<sub>3</sub>O<sub>2</sub>) is an azo dye with one azo group (-N=N-) used as a common pH indicator with  
 136 a *pKa* = 5.1. As other azo dyes, MR is a recalcitrant pollutant causing a significant burden on  
 137 the environment. The reduction of MR is known to be achieved with the cleavage of the azo  
 138 bond (Khalid *et al.*, 2008; Kone *et al.*, 2009), leading to the formation of two aromatic amines  
 139 (carboxyanilic acid: R<sub>1</sub>-NH<sub>2</sub> and *p*-dimethylaminoaniline: R<sub>2</sub>-NH<sub>2</sub>) as:



141 Thus, 4 Fe<sup>II</sup><sub>GR</sub> are theoretically needed to reduce MR and, assuming that GR is oxidized into  
 142 FeOOH, the reduction equations can be written as:







145

### 146 3. Materials and methods

147

#### 148 3.1. Chemicals

149 All solutions were prepared using ACS grade chemicals (except when specified) and 18.2  
150 M $\Omega$  cm N<sub>2</sub>-purged pure water (Purelab Option-Q, Elga LabWater, Antony, France). The  
151 mercury solution (750  $\mu$ M) was prepared from an HgCl<sub>2</sub> salt 99.5% (1166745, Merck) in HCl  
152 0.5 M (30721-2.5L, Sigma-Aldrich) and the pH was adjusted to  $7.0 \pm 0.1$  with NaOH 1M.  
153 Ferrous sulfate heptahydrate (FeSO<sub>4</sub>•7H<sub>2</sub>O, 99%), ferrous chloride tetrahydrate (FeCl<sub>2</sub>•4H<sub>2</sub>O,  
154 99%), and sodium phosphate (Na<sub>2</sub>HPO<sub>4</sub>•7H<sub>2</sub>O) were purchased from Sigma-Aldrich.  
155 Polyacrylic acid (C<sub>3</sub>H<sub>4</sub>O<sub>2</sub>)<sub>n</sub> was provided from a stock solution of 2 g L<sup>-1</sup> (Mw 2,000 g mol<sup>-1</sup>,  
156 Aldrich, 323667). The methyl red (C<sub>15</sub>H<sub>15</sub>N<sub>3</sub>O<sub>2</sub>) was provided by Sigma-Aldrich (98%,  
157 32654-25G).

158 The mercury concentration present in each reactant (0.3 – 1.9 ppb) was measured as blank  
159 (Table S1).

160

#### 161 3.2. Synthesis of GRs

162 Abiotically formed GRs were synthesized under O<sub>2</sub>-free conditions in an anaerobic  
163 chamber scavenging oxygen with palladium catalysts and H<sub>2</sub> (N<sub>2</sub>/H<sub>2</sub>, 95/5) (Coy Laboratory  
164 Products Inc.<sup>®</sup>). The GR1<sub>ab</sub> was obtained using a coprecipitation method as described by  
165 Bocher *et al.* (2004) by adding a mixture of Fe<sup>II</sup> and Fe<sup>III</sup> salts to a mixture of sodium  
166 hydroxide and sodium carbonate. Ferrous sulfate heptahydrate FeSO<sub>4</sub>•7H<sub>2</sub>O and ferric sulfate  
167 pentahydrate Fe<sub>2</sub>(SO<sub>4</sub>)<sub>3</sub>•5H<sub>2</sub>O were dissolved in 40 mL of pure water. A [Fe<sup>II</sup>]/[Fe<sup>III</sup>] ratio of  
168 2 was chosen with {[Fe<sup>II</sup>]+[Fe<sup>III</sup>]} = 0.5 M. Magnetic stirring (500 rpm) ensured fast and

169 complete dissolution. Di-sodium carbonate  $\text{Na}_2\text{CO}_3$  ( $[\text{CO}_3^{2-}] = 0.5 \text{ M}$ ) was dissolved in 40  
170 mL of a 1 M NaOH solution in order to have  $[\text{OH}^-]/\{[\text{Fe}^{\text{II}}]+[\text{Fe}^{\text{III}}]\} = 2$ . The carbonate  
171 solution was added to the solution of iron under the same conditions of magnetic stirring, and  
172 a bluish-green precipitate appeared immediately. GR1<sub>ab</sub> was used within a week of its  
173 formation to test its reactivity with  $\text{Hg}^{\text{II}}$  and MR, or was stabilized by addition of extra  
174  $\text{Na}_2\text{HPO}_4 \cdot 7\text{H}_2\text{O}$  salt  $\{[\text{PO}_4]_0/[\text{Fe}]\} = 0.8\%$  (*i.e.* 4 mM  $\text{PO}_4^{3-}$ ) (GR1<sub>ab+p</sub>) or silicic acid ( $\text{H}_4\text{SiO}_4$   
175 4 mM) (GR1<sub>ab+Si</sub>), or paa (500 mg L<sup>-1</sup>) (GR1<sub>ab+paa</sub>). A  $\{[\text{CO}_3^{2-}]/[\text{SO}_4^{2-}]\}$  ratio of 1 was chosen  
176 to prevent the formation of sulfate GR2<sub>ab</sub> as described by Bocher *et al.* (2004).

177 The abiotic sulfate GR2 (GR2<sub>ab</sub>) was synthesized using the coprecipitation method  
178 developed by Ruby *et al.* (2003). Briefly, 20 millimoles of an iron solution, containing 13.3  
179 millimoles  $\text{Fe}^{\text{II}}$  (3.7 g of  $\text{FeSO}_4 \cdot 7\text{H}_2\text{O}$ ) and 6.7 millimoles  $\text{Fe}^{\text{III}}$  (1.63 g of  $\text{Fe}_2(\text{SO}_4)_3 \cdot 5\text{H}_2\text{O}$ ),  
180 were added to 400 mL of pure water. Iron salts were precipitated by addition of NaOH (50  
181 mL, 40 mM) with a syringe and under magnetic stirring to precipitate all the iron salts  
182 ( $n\text{NaOH} / n\text{Fe} = 2$ ).

183 The biotic carbonate GR1 (GR1<sub>bio</sub>) was produced according to Zegeye *et al.* (2007) by  
184 incubation of *S. putrefaciens* CIP 8040<sup>T</sup> ( $2.5 \times 10^9$  cells mL<sup>-1</sup>) at 30°C in a basal medium  
185 containing 160 mM of sodium formate ( $\text{HCOONa}$ ) and 300 mM of lepidocrocite ( $\gamma\text{-FeOOH}$ )  
186 as the sole electron donor and acceptor, respectively.

187 All GRs synthesized were washed in O<sub>2</sub>-free deionized water by centrifugation (5 min,  
188  $10,000 \times g$ ) and the concentration of GRs was determined by the spectrophotometric ferrozine  
189 method measuring the concentration of  $\text{Fe}^{\text{II}}$  and  $\text{Fe}^{\text{total}}$  (Viollier *et al.*, 2000) after HCl  
190 extraction (6 M) in a Tecan Infinite M200 PRO microplate reader. GRs were characterized by  
191 X-ray diffraction (XRD), transmission electron microscopy (TEM), and transmission  
192 Mössbauer spectroscopy (TMS).

193

### 194 3.3. Experimental set-up of Hg<sup>II</sup> and methyl red reduction by GRs

195 The Hg<sup>II</sup> solution (5  $\mu$ M, initial starting concentration) was introduced into a 250 mL  
196 glass reactor (borosilicated glass, Schott) containing 150 mL of pure water with a GR  
197 suspension (500  $\mu$ M, Hg/GR = 1/100). Initially, the glass reactor pH was adjusted to 7.0, 8.2,  
198 and 9.5 with NaOH 1N or HCl 0.5N. The glass reactor was continuously N<sub>2</sub>-purged and  
199 stirred (300 rpm) in order to outgas Hg<sup>0</sup> and prevent any oxidation from ambient air. One  
200 milliliter of the unfiltered suspension (*i.e.* with dissolved and adsorbed Hg) was sampled at  
201 regular time intervals and was immediately dissolved in an acidic solution of HNO<sub>3</sub>/HCl (500  
202  $\mu$ L HNO<sub>3</sub> at 65% with 500  $\mu$ L HCl at 30%, w/v), before being diluted ten times. This acidic  
203 digestion was performed in order 1) to stop the reaction and preserve the mercury speciation,  
204 and 2) to dissolve the mineral phase and to release the potential adsorbed Hg fraction in the  
205 aqueous phase. Thus, the potential adsorption of Hg on GR surfaces should not bias the  
206 determination of reduction kinetic. Moreover, the formation of Hg<sup>0</sup> was qualitatively checked  
207 by trapping it during the reaction between Hg<sup>II</sup> species and green rust in a solution of KMnO<sub>4</sub>  
208 50 mM (in H<sub>2</sub>SO<sub>4</sub> 10%), where the elemental volatile mercury was re-oxidized into Hg<sup>II</sup>  
209 under acidic conditions (data not shown).

210 The methyl red (MR) solution was prepared in pure water and the pH was adjusted to  
211  $7.0 \pm 0.1$  with NaOH 1N. The MR solution (final concentration  $\sim 15 \mu$ M) was introduced in a  
212 glass batch reactor containing 150 mL of pure water with a GR suspension (500  $\mu$ M, MR/GR  
213  $\sim 1/33$ ). During the reaction, the medium was continuously stirred (300 rpm) and 1 mL  
214 samples were removed over time after adjusting the pH to  $7.0 \pm 0.1$  in order to avoid shifting  
215 the maximum peak (at 430 nm).

216 Control experiments were also carried out for Hg<sup>II</sup> and MR on the same terms as before,  
217 respectively. The Fe<sup>II</sup><sub>aq</sub> control was performed (0.2 mM, pH 7) to assess the reactivity of Hg<sup>II</sup>  
218 or MR with aqueous Fe<sup>II</sup> *versus* structural Fe<sup>II</sup>. Such amounts of Fe<sup>II</sup> were chosen assuming

219 that  $\sim 0.2$  mM of  $\text{Fe}^{\text{II}}_{\text{aq}}$  (*i.e.* passing through  $0.2 \mu\text{m}$ ) was measured in a suspension of GR (not  
220 shown). A bacterial control with  $6 \times 10^5$  cells  $\text{mL}^{-1}$  of *S. putrefaciens* was performed to  
221 evaluate the effect of bacteria in the GR1<sub>bio</sub> suspension. The cell density selected was similar  
222 to what is required for  $500 \mu\text{M}$  GR1<sub>bio</sub>.

223

#### 224 3.4. Analyses

225 The Hg concentration was determined with a Milestone DMA-80 Direct Mercury  
226 Analyzer (Milestone GmbH, Germany). Its unique processing of samples by thermal  
227 decomposition, amalgamation, and atomic absorption spectrometry provides a direct analysis  
228 of the sample matrices.

229 The MR concentration was measured by a spectrophotometric analytical method (Cary  
230 60 UV-Vis, Agilent Technologies). A broad band in the visible MR spectrum was  
231 characterized at  $430 \text{ nm}$  in pH 7 (Fig. S1) and was assigned to the azo band (Hou *et al.*, 2007).  
232 To avoid artifacts caused by suspended particles, short centrifugations were performed (2 min,  
233  $14,000 \times g$ ) before determining MR concentration. The sorption of MR by GR was not  
234 considered here, as we assumed it to be negligible as previously shown (Kone *et al.*, 2009).

235 XRD data were collected with a D8 Bruker diffractometer, equipped with a  
236 monochromator and a position-sensitive detector. The X-ray source was a Co anode ( $k =$   
237  $0.17902 \text{ nm}$ ). The diffractogram was recorded in the  $3\text{-}64$   $2\theta$  range, with a  $0.0359^\circ$  step size  
238 and collecting time of 3 s per point.

239 TMS analyses were performed using a constant-acceleration spectrometer with a 50  
240 mCi source of  $^{57}\text{Co}$  in Rh. The spectrometer was calibrated with a  $25 \mu\text{m}$  foil of  $\alpha$ -Fe at  
241 room temperature. The cryostat consisted of a closed cycle helium Mössbauer cryogenic  
242 workstation with vibration isolation stand manufactured by Advance Research Systems®.  
243 Helium exchange gas was used to thermally couple the sample to the refrigerator, allowing

244 variable temperature operations from 7 to 300 K. Computer fittings were done using  
245 Lorentzian-shape lines.

246 Transmission electron microscopy was conducted using CM20/STEM Philips coupled  
247 with an energy dispersive X-ray system (EDX) using a voltage of 200 kV. One drop of the  
248 suspension was laid on an amorphous carbon-coated grid and loaded into the analysis holder  
249 of the microscope under  $10^{-8}$  Torr vacuum.

250 The surface area of GRs was determined by multipoint  $N_2$ -BET analysis using a Coulter  
251 (SA113) surface area analyzer. Prior to specific surface area determination, GR suspensions  
252 were dried by vacuum desiccation for 48 h.

253

## 254 **4. Results and discussion**

### 255 **4.1. Characterization of GRs**

256 The greenish solid phase formed by either the microbial reduction of lepidocrocite ( $\gamma$ -  
257 FeOOH) by *S. putrefaciens* or chemical synthesis was characterized by XRD (Fig. 1a) and the  
258 d-values obtained were summarized in Table S2. The carbonate GR1 was identified as a  
259 major secondary iron mineral produced by the bacterial activity (GR1<sub>bio</sub>) and as a main  
260 product from the coprecipitation method in the presence of carbonate and stabilized with  
261 phosphate (GR1<sub>ab+P</sub>) or not stabilized (GR1<sub>ab</sub>), which is in close agreement with previous  
262 studies (Drissi *et al.*, 1995; Zegeye *et al.*, 2007). TEM images and electron diffraction  
263 patterns were also performed and hexagonal crystals of GR1 were observed in various sizes  
264 from 5  $\mu\text{m}$  to 10  $\mu\text{m}$  for GR1<sub>bio</sub> and from 100 nm to 300 nm for GR1<sub>ab+P</sub> (Fig. 1b, c and d).  
265 This is consistent with the values reported in previous investigations (Ona-Nguema *et al.*,  
266 2002; Zegeye *et al.*, 2014).

267 The formation of hydroxysulfate GR2 (GR2<sub>ab</sub>) by the coprecipitation method from  
268 Ruby *et al.* (2003) was confirmed both by the d-values from the XRD diffractogram and by

269 the electron diffraction pattern, which is in agreement with the literature (Simon *et al.*, 1997)  
270 (Fig. 1, Table S2). Hexagonal particles of GR2<sub>ab</sub> were observed by TEM with sizes ranging  
271 from 200 to 400 nm, which is in line with what Zegeye *et al.* (2005) had reported.

272 All the GRs formed were quasi-free of crystallographic impurities at a discernible level  
273 of XRD (Fig. S2). The Fe<sup>II</sup>/Fe<sup>III</sup> ratio was determined by TMS or by ferrozine method on  
274 solids (Fig. S3, Table S3): 1.2 (GR1<sub>ab+p</sub>) ≤ 1.6 (GR1<sub>bio</sub>) ≤ 2.0 (GR2<sub>ab</sub>) ≤ 2.2 GR1<sub>ab</sub>, and the  
275 specific surface area (SSA) was also measured by N<sub>2</sub>-BET analysis (Table 1): 13 m<sup>2</sup> g<sup>-1</sup>  
276 (GR1<sub>bio</sub>) ≤ 14 ± 2 m<sup>2</sup> g<sup>-1</sup> (GR2<sub>ab</sub>) ≤ 31 ± 6 m<sup>2</sup> g<sup>-1</sup> (GR1<sub>ab+p</sub> and GR1<sub>ab</sub>) and also expressed as  
277 surface area concentration (A) in Table 1. These SSA values of green rusts were slightly lower  
278 than those obtained by Williams and Scherer (2001): 47 ± 7 m<sup>2</sup> g<sup>-1</sup>. This fluctuation of SSA of  
279 green rusts depends on the synthesis method, which influences the crystal size. Moreover, the  
280 delay between its synthesis and its use modifies the crystal size probably by an Ostwald  
281 ripening.

282 Having determined SSA for each GR, the concentration of the surface Fe<sup>II</sup> sites  
283 available can be reasonably estimated since the reactivity of GRs is based on this value. Here,  
284 an example is given for GR1<sub>bio</sub> with an initial concentration of 500 μM and with the A value  
285 of 4.2 m<sup>2</sup> L<sup>-1</sup> (Table 1). Knowing that the average common value of the surface site density is  
286 5 Fe<sup>II</sup> sites per nm<sup>2</sup> for iron oxides (Williams and Scherer, 2001), the number of Fe<sup>II</sup> sites per  
287 nm<sup>2</sup> and per L of GR1<sub>bio</sub> was determined at 2.1 × 10<sup>19</sup> Fe<sup>II</sup> sites nm<sup>-2</sup> L<sup>-1</sup> (i.e. 5 Fe<sup>II</sup> sites nm<sup>-2</sup> ×  
288 4.2 × 10<sup>18</sup> nm<sup>2</sup> L<sup>-1</sup>). The total concentration of Fe<sup>II</sup> sites on GR1<sub>bio</sub> surface was therefore  
289 estimated at 34.8 μM (Table 1).

#### 290 4.2. Kinetics of Hg<sup>II</sup> reduction by GRs

291 Regardless the GR species, the Hg<sup>II</sup> concentrations decreased rapidly according to an  
292 exponential decay at neutral and alkaline pH values (7.0, 8.2, and 9.5) (Fig. 2). Since GRs  
293 were present in great excess, their concentrations are assumed to have been constant

294 throughout the reaction and the decrease in Hg concentration can be described by a pseudo  
 295 first-order reaction (equations 8, 9):

$$296 \quad d[\text{Hg}]_t/dt = -k_{\text{obs}} \times [\text{Hg}]_t \quad (8)$$

$$297 \quad [\text{Hg}]_t = [\text{Hg}]_0 \times \exp(-k_{\text{obs}} \times t) \quad (9)$$

298 where  $k_{\text{obs}}$  is the pseudo first-order rate constant ( $\text{min}^{-1}$ ), and  $[\text{Hg}]_t$  and  $[\text{Hg}]_0$ , the total  
 299 concentrations of cationic mercury at time  $t$  and  $0$ , respectively. The fitting by a pseudo first-  
 300 order reaction is consistent with other studies with GR and various oxidants such as selenite,  
 301  $\text{CCl}_4$ , nitrate, and  $\text{Cr}^{\text{VI}}$  (Erbs *et al.*, 1999; Hansen *et al.*, 2001; Williams and Scherer, 2001;  
 302 Etique *et al.*, 2014b). The values of  $k_{\text{obs}}$  were determined from equation (9) by plotting –  
 303  $\ln([\text{Hg}]_t/[\text{Hg}]_0)$  as a function of time  $t$ . To take into account the  $\text{Fe}^{\text{II}}$  content of GRs (Note S1),  
 304  $k_{\text{obs}}$  values were normalized to  $\text{Fe}^{\text{II}}$  content ( $k_{\text{Fe}^{\text{II}}}$ ,  $\text{L mmol}^{-1} \text{min}^{-1}$ ) (Note S2), but it does not  
 305 significantly affect the hierarchy as regards the kinetic rate constants (Table 1). Similarly, a  
 306  $k_{\text{obs}}$  normalization to the concentration of  $\text{Fe}^{\text{II}}$  sites on the green rust surface ( $k_{\text{S}}$ ,  $\text{L mmol}^{-1}$   
 307  $\text{min}^{-1}$ ) (Note S3) does not seem to influence significantly the decrease of the Hg reduction rate  
 308 from pH 7.0 to pH 9.5 (Table 1). However, at pH 8.2 the  $k_{\text{S}}$  values clearly highlight the  
 309 increase of Hg reduction kinetics when  $\text{Hg}^{\text{II}}/\text{GR}$  ratio increases from 1/80 to 1/0.8 for GR1<sub>bio</sub>  
 310 and from 1/100 to 1/10 for GR1<sub>ab</sub> (Table 1, Fig. S4). Thus, this approach with  $k_{\text{S}}$  appeared to  
 311 be more relevant compared to the expressions of kinetics rate constants in  $k_{\text{obs}}$  and  $k_{\text{Fe}^{\text{II}}}$ .

312 Control tests were performed with aqueous  $\text{Fe}^{\text{II}}$  (0.2 mM, pH = 7.0) or with bacteria (pH  
 313 = 7.0) and no significant decrease in Hg concentration was observed over time ( $k_{\text{obs}} < 10^{-3}$   
 314  $\text{min}^{-1}$ ) (Fig. S5a). This indicates that the depletion of Hg is neither due to a reduction reaction  
 315 with the aqueous  $\text{Fe}^{\text{II}}$ , nor to sorption on glass walls. Similarly, bacteria associated with  
 316 GR1<sub>bio</sub> do not appear to be responsible for the  $\text{Hg}^{\text{II}}$  decrease. Thus, *S. putrefaciens* is not able,  
 317 in our experimental conditions, to reduce  $\text{Hg}^{\text{II}}$ . It is worth noting that other iron reducers such  
 318 as *S. oneidensis* MR-1 or *Geobacter* spp are able to reduce  $\text{Hg}^{2+}$  especially with lower

319 amounts of  $\text{Hg}^{\text{II}}$  ( $0.15 \mu\text{M}$ ) and under growth conditions (Wiatrowski *et al.* 2006). In the  
320 present work, *S. putrefaciens* was in stationary growth phase and no electron donor or carbon  
321 source were added (non-growth conditions).

322 These results demonstrate that GRs reduced effectively  $\text{Hg}^{\text{II}}$  to  $\text{Hg}^0$ . Compared to other  
323  $\text{Fe}^{\text{II}}$  solids, these reaction kinetics are of the same order of magnitude as those induced by  
324 magnetite (Wiatrowsky *et al.*, 2006) or by the  $\text{Fe}^{\text{II}}$  species sorbed onto phlogopite (Charlet *et*  
325 *al.*, 2002). O'Loughlin *et al.* (2003) have reported slightly higher rates of  $\text{Hg}^{\text{II}}$  reduction by  
326 GR2, as they reduced 98.7% of the initial  $\text{Hg}^{\text{II}}$  ( $6.4 \text{ mmol L}^{-1}$  of GR2<sub>ab</sub> with  $400 \mu\text{mol L}^{-1} \text{Hg}^{\text{II}}$ ,  
327  $\text{GR}/\text{Hg}^{\text{II}} = 16$ ) after 30 min. Here, we report a thorough reduction of  $\text{Hg}^{\text{II}}$  in less than an hour  
328 (with a ratio 6 times higher  $\text{GR}/\text{Hg}^{\text{II}} = 100$  as compared to O'Loughlin *et al.*, 2003).  
329 Nevertheless, it cannot be excluded that part of  $\text{Hg}^0$  could still be trapped in the solid phase,  
330 which would underestimate the kinetics of  $\text{Hg}^{\text{II}}$  reduction (Pasakarnis *et al.*, 2013).

#### 331 **4.2.1. Evolution of the $\text{Fe}^{\text{II}}$ concentration and determination of the stoichiometry of the** 332 **reduction of $\text{Hg}^{\text{II}}$ species by GRs**

333 The green rust reactivity was also evaluated by measuring the evolution of the total  $\text{Fe}^{\text{II}}$   
334 concentration of the suspension. Among all experiments, only 3 runs present a detectable  
335 decrease of the  $\text{Fe}^{\text{II}}/\text{Fe}_{\text{tot}}$  ratio in the presence of  $\text{Hg}^{\text{II}}$  species for a ratio  $\text{Hg}^{\text{II}}/\text{GR}$  of 1/10  
336 (GR1<sub>ab</sub>) (Fig. S4a), 1/8 and 1/0.8 (GR1<sub>bio</sub>) (Fig. S4b). For all the other experiments, the  $\text{Fe}^{\text{II}}$   
337 concentration did not vary significantly since GR was used in large excess in comparison to  
338 the initial amount of  $\text{Hg}^{\text{II}}$  species ( $5 \mu\text{M}$ ). During the reduction of mercury, the  $\text{Fe}^{\text{II}}/\text{Fe}_{\text{tot}}$  ratio  
339 lowered of 0.06 units for GR1<sub>ab</sub> (1/10) and GR1<sub>bio</sub> (1/8) (Fig. S4). However, a sharp decrease  
340 from 0.67 to 0.46 was noted for the 1/0.8 ratio of  $\text{Hg}^{\text{II}}/\text{GR1}_{\text{bio}}$  (Fig. S4b). Thus,  $\text{Fe}^{\text{II}}$  species of  
341 GR were oxidized to  $\text{Fe}^{\text{III}}$  species during the reduction of  $\text{Hg}^{\text{II}}$  species, and this chemical  
342 observation was confirmed by the characterization of magnetite as end product (Fig. S6).



343 Moreover, the stoichiometry of the reaction between  $\text{Fe}^{\text{II}}$  species and  $\text{Hg}^{\text{II}}$  species was  
344 determined at 1/10, 1/8 and 1/0.8 ratios of  $\text{Hg}^{\text{II}}/\text{GR}$  (Fig. 3). The expected ratio  $\text{Hg}^{\text{II}}:\text{Fe}^{\text{II}}_{\text{GR}}$   
345 corresponding to the amount of consumed  $\text{Hg}^{\text{II}}$  ions over the amount of oxidized  $\text{Fe}^{\text{II}}$  species  
346 during the reduction of mercury by green rust is 1:2 according to the equation (3). This  
347 theoretical ratio of  $\text{Hg}^{\text{II}}:\text{Fe}^{\text{II}}_{\text{GR}}$  was confirmed by the determination of the 1:1.9 experimental  
348 ratio (Fig. 3). Thus, this is in agreement (95 %) with the stoichiometry of the reaction  
349 involving the oxidation of 2 moles of ferrous iron per 1 mole of  $\text{Hg}^{\text{II}}$  reduced species.

#### 350 4.2.2. Effect of pH on GR reactivity

351 In aqueous systems, GR particles act as Lewis acid and coordinate water or hydroxyl  
352 groups. This is why the particles surface chemistry is highly dependent of pH value. Recently,  
353 the point of zero charge (pzc) of GRs (GR1 and GR2) has been accurately determined at  
354  $8.3 \pm 0.1$  (Guilbaud *et al.*, 2013). Therefore, at  $\text{pH} < 8.3$ , the surface of GR particles is  
355 protonated, leading to a positive surface charge (Fig. 4); at  $\text{pH} > 8.3$ , the GR surface is  
356 negatively charged (Fig. 4). The evolution of the net surface charge of GR with pH may affect  
357 the rate and the extent of the reduction of contaminants such as chromate or mercury.  
358 Williams and Scherer (2001) demonstrated that the reduction of anionic pollutants such as  
359  $\text{CrO}_4^{2-}$  was enhanced by a sorption onto positively charged surface of GR. Thus, the most  
360 significant reduction of  $\text{Hg}^{\text{II}}$  should be expected for a negatively charged surface of GRs ( $\text{pH}$   
361  $> 8.3$ ), where the electrostatic interactions are more favorable for  $\text{Hg}^{2+}$  sorption.

362 However, the predominant phase of mercury at pH of this study is  $\text{Hg}(\text{OH})_2$  (Fig. 4). At  
363 all tested pH values and whatever GRs used ( $\text{GR}_{2\text{ab}}$ ,  $\text{GR}_{1\text{bio}}$ , and  $\text{GR}_{1\text{ab+p}}$ ), the highest value  
364 of  $k_{\text{obs}}$  ( $\sim 4 \times 10^{-2} \text{ min}^{-1}$ ) was obtained at pH 7.0, when GRs have a positive surface charge (Fig.  
365 2a, Table 1). This would suggest, as it was previously considered for the reaction of magnetite  
366 with  $\text{Hg}^{\text{II}}$  (Wiatrowsky *et al.*, 2009), that hydroxyl groups of  $\text{Hg}(\text{OH})_2$  could react with  
367 protonated GR particles, thus enhancing the sorption of mercury at the surface of GR

368 followed by a reduction into  $\text{Hg}^0$ . Indeed, when pH values rise from 7.0 to 8.2 (or 9.5), the  
369 values of  $k_{\text{obs}}$  for  $\text{GR1}_{\text{ab+P}}$ ,  $\text{GR1}_{\text{bio}}$ , and  $\text{GR2}_{\text{ab}}$  decrease by a factor of ~20%, 30%-50%, and  
370 60%-70%, respectively (Table 1). GR reactivity at alkaline pH can be ranked as:  $\text{GR1}_{\text{ab+P}} >$   
371  $\text{GR1}_{\text{bio}} > \text{GR2}_{\text{ab}}$ . No significant difference in  $k_{\text{obs}}$  values was noted for each type of GRs  
372 between pH 8.2 and 9.5 (Table 1). Thus, the reduction of  $\text{Hg}(\text{OH})_2$  by GR would be favored  
373 at  $\text{pH} < 8.3$  (Fig. 4). Therefore, the fluctuation of the surface charge of GR in the function of  
374 pH governs the adsorption of  $\text{Hg}(\text{OH})_2$  and its reduction.

375 Coupled with the adsorption/reduction of  $\text{Hg}(\text{OH})_2$ , a decrease in pH was observed for  
376 the reaction with  $\text{GR2}_{\text{ab}}$ , whereas pH values remained almost constant with  $\text{GR1}_{\text{bio}}/\text{GR1}_{\text{ab+P}}$   
377 (Table S4). These observations are consistent with equations (5) and (6), since the reduction  
378 of  $\text{Hg}^{\text{II}}$  is associated with the production of two  $\text{H}^+$  for  $\text{GR2}$  instead of one  $\text{H}^+$  for  $\text{GR1}$  (due to  
379 the presence of bicarbonate at the pH range values investigated).

#### 380 4.2.3. Minor impact of cells and phosphate on the $\text{Hg}^{\text{II}}$ reduction

381 Phosphate and bacterial cells (as bacterial bodies with polymeric substances) are known  
382 to improve the stability of GRs (Bocher *et al.*, 2004; Jorand *et al.*, 2013) and to affect their  
383 reactivity towards nitrate (Etique *et al.*, 2014b; Zegeye *et al.*, 2014). To test whether these  
384 stabilizing agents would affect the reactivity of the studied GRs towards  $\text{Hg}^{\text{II}}$ , experiments  
385 were performed with and without bacterial cells or phosphate, and the rate and the extent of  
386 the  $\text{Hg}^{\text{II}}$  reduction were determined. When  $\text{GR2}_{\text{ab}}$  was supplemented with *S. putrefaciens* cells  
387 ( $\text{GR2}_{\text{ab+cells}}$ ),  $k_{\text{S}}$  did not significantly change compared to  $\text{GR2}_{\text{ab}}$  (Fig. 2, Table 1). Similarly,  
388 no significant difference was noted between  $\text{GR1}_{\text{ab}}$  and  $\text{GR1}_{\text{ab+P}}$  (*i.e.*  $\text{GR1}$  supplemented with  
389 0.8% phosphate) (Fig. 2b, Table 1). Therefore, bacterial cells or phosphates have a minor  
390 impact on the reactivity of GRs towards  $\text{Hg}^{\text{II}}$ , and the  $\text{GR1}_{\text{bio}}$  can reduce  $\text{Hg}^{\text{II}}$  as effectively as  
391  $\text{GR1}_{\text{ab}}$ . This suggests that *S. putrefaciens* did not inhibit significantly the reduction of  $\text{Hg}^{\text{II}}$  by  
392 GRs as it has already been shown for other bacteria (Mishra *et al.*, 2011).

### 393 4.3. Kinetics of methyl red reduction by GRs

394 Here also, the reaction kinetics can be described by a pseudo first-order reaction  
395 (equations 10, 11):

$$396 \quad d[\text{MR}]_t/dt = -k_{\text{obs}} \times [\text{MR}]_t \quad (10)$$

$$397 \quad [\text{MR}]_t = [\text{MR}]_0 \times \exp(-k_{\text{obs}} \times t) \quad (11)$$

398 where  $k_{\text{obs}}$  is the pseudo first-order rate constant ( $\text{min}^{-1}$ ), and  $[\text{MR}]_t$  and  $[\text{MR}]_0$  the total  
399 concentrations of MR at time  $t$  and  $0$ , respectively. However, it should be noted that a certain  
400 number of kinetic curves present a latency time (slight sigmoidal shape) (GR1<sub>ab+Si</sub> and  
401 GR1<sub>ab+paa</sub>, Fig. 5), and a better description of this lag-time merits to be investigated in further  
402 studies.

403 The values of  $k_{\text{obs}}$  were determined from equation (11) by plotting  $-\ln([\text{MR}]_t/[\text{MR}]_0)$  as a  
404 function of time  $t$  (Table 2). The  $\text{Fe}^{\text{II}}$  content of GRs and the concentration of  $\text{Fe}^{\text{II}}$  sites on the  
405 green rust surface were also taken into account to normalize  $k_{\text{obs}}$  values and to define  $k_{\text{Fe}^{\text{II}}}$   
406 ( $\text{L min}^{-1} \text{mmol}^{-1}$ ) and  $k_S$  ( $\text{L mmol}^{-1} \text{min}^{-1}$ ), but it does not significantly affect the hierarchy as  
407 regards the kinetic rate constants (Table 2).

408 MR was completely reduced by GR2<sub>ab</sub> in less than 30 min with a  $k_S$  value of 3.4  
409  $\text{L mmol}^{-1} \text{min}^{-1}$  ( $t_{1/2} = 5$  min) (Fig. 5). Generally, all the GRs used showed lower  $k_S$  values than  
410 those obtained for  $\text{Hg}^{\text{II}}$  reduction (except for the  $\text{Hg}^{\text{II}}$ /GR ratios of 1/10, 1/8 and 1/0.8). For  
411 example, MR was fully reduced by GR1<sub>ab</sub> in 120 min (Fig. 5) instead of only 60 min for a  
412 total reduction of  $\text{Hg}^{\text{II}}$  ( $\text{Hg}^{\text{II}}$ /GR ratio of 1/100) (Fig. 2a). However,  $k_S$  obtained for a reaction  
413 of MR with GR1<sub>bio</sub> had a significantly lower value ( $0.057 \text{ L mmol}^{-1} \text{min}^{-1}$ ) (Table 2) when  
414 compared to the reaction between GR1<sub>bio</sub> (1/80) and  $\text{Hg}^{\text{II}}$  ( $k_{\text{obs}} = 1.18 \text{ mmol}^{-1} \text{min}^{-1}$ ) (Table 1).  
415 Thus, the time needed to reduce MR by GR1<sub>bio</sub> (1200 min) (Fig. 5) is 20 times higher than for  
416 the reduction of  $\text{Hg}^{\text{II}}$  (60 min) (Fig. 2a).

#### 417 4.3.1. Critical role of bacterial cells and phosphate on MR reduction

418 Since *Shewanella* spp. were shown to degrade MR (Khalid *et al.*, 2008), the degradation  
419 of MR by GR1<sub>bio</sub> could be due to an active metabolism of cells involved in the GR1<sub>bio</sub>  
420 formation and remaining in the mineral suspension. To assess the effect of *S. putrefaciens* on  
421 MR removal, a series of batch experiments were performed with a fresh cell suspension in the  
422 same physiological state (late stationary phase), and with a heat inactivated suspension. In  
423 both cases, no significant decrease in MR levels was obtained indicating that cells present  
424 with GR<sub>bio</sub> do not contribute to MR removal (Fig. S5b).

425 To test whether bacteria could affect the reactivity of GRs, *Shewanella* cells were added  
426 to GR2<sub>ab</sub>, the most reactive GR (high  $k_S$ ). A significant decrease in the MR reduction rate by a  
427 factor of 200 was observed relative to GR2<sub>ab</sub> (Table 2, Fig. 5), which indicates that bacterial  
428 cells inhibit considerably the MR reduction by GRs. Similarly,  $k_S$  of GR1<sub>ab+P</sub> was ~200 times  
429 lower than that of GR2<sub>ab</sub> ( $0.007 \text{ L mmol}^{-1} \text{ min}^{-1}$  and  $3.4 \text{ L mmol}^{-1} \text{ min}^{-1}$ , respectively, Table  
430 2), thereby underscoring that phosphates impaired significantly the reactivity of GR. This is in  
431 line with a recent work dealing with the effect of phosphates on the reduction of nitrate by GR  
432 (Etique *et al.*, 2014b).

### 433 **4.3.2. A moderate inhibition of GRs reactivity towards MR by silicate and polyacrylic** 434 **acid**

435 To investigate whether other environmentally relevant components could affect GR  
436 reactivity, experiments were performed with  $\text{H}_4\text{SiO}_4$  and paa. Such compounds can represent  
437 (or be models of) aqueous Si from quartz associated with soil particles or extra-cellular  
438 polymeric substances from biofilms (Sergent *et al.*, 2011; Jorand *et al.*, 2013). The  $k_S$  of  
439 GR1<sub>ab+Si</sub> and GR1<sub>ab+paa</sub> ( $0.156 \text{ L mmol}^{-1} \text{ min}^{-1}$  and  $0.193 \text{ L mmol}^{-1} \text{ min}^{-1}$ , respectively) were  
440 ~20 times higher than that of GR1<sub>ab+P</sub> and ~10 times lower than that of GR2<sub>ab</sub> (Table 2, Fig.  
441 5). This result is in line with a recent study pointing out that GR1 stabilized with EPS  
442 (GR1<sub>ab+paa</sub>) is quasi-unreactive towards nitrate (Zegeye *et al.*, 2014). Thus, it implies that paa,

443  $\text{H}_4\text{SiO}_4$ , and cells would have a less pronounced “screen effect” than phosphate, or be sorbed  
444 onto different reactive sites as compared to MR.

445 As stated before, the stoichiometric difference ( $\text{Fe}^{\text{II}}/\text{Fe}^{\text{III}}$ ) between GRs could influence  
446 the rate of reduction, as well as the concentration of surface  $\text{Fe}^{\text{II}}$  site of GR. However, even  
447 considering  $k_s$  or  $k_{\text{FeII}}$ , the hierarchy of GR reactivity with MR remains unchanged (Table 2):

448  $k_s(\text{GR1}_{\text{ab+P}}) < k_s(\text{GR2}_{\text{ab+cells}}) < k_s(\text{GR1}_{\text{bio}}) < k_s(\text{GR1}_{\text{ab+Si}}) < k_s(\text{GR1}_{\text{ab+paa}}) < k_s(\text{GR1}_{\text{ab}}) < k_s(\text{GR2}_{\text{ab}})$ .

449 To know whether MR was effectively reduced and not only sorbed onto the solid phase,  
450 the presence of degradation products from MR reduction was checked. At the end of the  
451 reduction, the main absorption peak at 430 nm had disappeared while a band in the ultraviolet  
452 region at 305 nm had increased (Fig. S1). This absorbance band in the UV region could be  
453 assigned to the presence of *p*-dimethylaminoaniline. This result is consistent with equation (5),  
454 as well as with the findings of Hou *et al.* (2007) and Kone *et al.* (2009) who reported that  
455 methyl orange and methyl red were reduced by zero-valent iron and  $\text{GR2}_{\text{ab}}$ , respectively,  
456 through cleavage of the azo bond into sulfanilic or carboxyanilic acid and *p*-  
457 dimethylaminoaniline. Control with aqueous  $\text{Fe}^{\text{II}}$  was performed and no reduction of MR was  
458 observed (Fig. S5b).

#### 459 4.4. MR and $\text{Hg}^{\text{II}}$ reduction mechanisms by GRs

##### 460 4.4.1. Estimation of the number of moles of contaminant that could be reduced by GRs

461 The number of moles of  $\text{Hg}^{\text{II}}$  species or MR that could be reduced for a given surface  
462 area of GR at the given pH value can only be determined for a run highlighting an incomplete  
463 consumption of the contaminant. Thus, the initial concentration of GR used during the  
464 reduction of the pollutant has not to be sufficient to fully reduce the initial amount of  $\text{Hg}^{\text{II}}$   
465 species or MR. This phenomenon is described by the term saturation.

466 Additional experiment was carried out, where  $\text{Hg}^{\text{II}}$  species were added successively to  
467 the  $\text{GR1}_{\text{bio}}$  suspension (400  $\mu\text{M}$ ) in quantities of 5  $\mu\text{M}$  to 100  $\mu\text{M}$  to reach a final  $\text{Hg}^{\text{II}}$

468 concentration of 130  $\mu\text{M}$  in the reaction medium (pH 8.2) (Fig. 6). One day after the  
469 beginning of the reaction, the quantity of  $\text{Hg}^{\text{II}}$  removed was 77  $\mu\text{M}$  (Fig. 6), representing  
470 59 % of the total addition of  $\text{Hg}^{\text{II}}$ . Between each addition of  $\text{Hg}^{\text{II}}$ , the kinetics of the reaction  
471 decreased (first addition:  $k_{\text{obs},\#1} = 4.1 \pm 0.1 \times 10^{-2} \text{ min}^{-1}$ ; third addition:  $k_{\text{obs},\#3} = 1.6 \pm 0.2 \times 10^{-2}$   
472  $\text{ min}^{-1}$ ; last addition:  $k_{\text{obs},\#5} = 5.0 \times 10^{-4} \text{ min}^{-1}$ ) suggesting that the availability of  $\text{Fe}^{\text{II}}$  sites on  
473 the surface of  $\text{GR1}_{\text{bio}}$  lowered. However, all the  $\text{Fe}^{\text{II}}$  sites on the  $\text{GR1}_{\text{bio}}$  surface do not seem to  
474 be saturated with a  $\text{Hg}^{\text{II}}/\text{GR}$  ratio of 1/5.2 (i.e. 77/400). This ratio was increased in another  
475 additional run performed with a  $\text{Hg}^{\text{II}}/\text{GR}$  ratio of 1/0.8 at pH 8.2. A plateau was reached at  
476 1.66  $\mu\text{M}$  (Fig. S4b), evidencing a partial reduction of mercury with an initial concentration of  
477  $\text{GR1}_{\text{bio}}$  of 4  $\mu\text{M}$ . Here, a saturation was highlighted and the amount of  $\text{Hg}^{\text{II}}$  species reduced by  
478 surface area concentration of  $\text{GR1}_{\text{bio}}$  was estimated at  $1.1 \times 10^{-4}$  moles of  $\text{Hg}^{\text{II}} \text{ m}^{-2}$ .

479 For the reduction of MR, none of our carried out experiments showed an incomplete  
480 consumption of  $\text{C}_{15}\text{H}_{15}\text{N}_2\text{O}_3$  species at pH 7 (Fig. 5). Nevertheless, we can estimate the  
481 minimum amount of  $\text{C}_{15}\text{H}_{15}\text{N}_2\text{O}_3$  species that can be reduced by  $\text{GR1}_{\text{bio}}$  at  $4.3 \times 10^{-6}$  moles of  
482  $\text{MR m}^{-2}$  or more.

#### 483 4.4.2. Parameters influencing the kinetics of the MR reduction vs the $\text{Hg}^{\text{II}}$ reduction

484 The MR reaction kinetics were more affected in the presence of GR stabilizing agents,  
485 such as phosphate or bacterial cells, than the reduction of  $\text{Hg}^{\text{II}}$  ( $\text{GR2}_{\text{ab+p}}/\text{Hg}^{\text{II}}$  and  
486  $\text{GR2}_{\text{ab+cells}}/\text{Hg}^{\text{II}}$ , Fig. 2a;  $\text{GR2}_{\text{ab+p}}/\text{MR}$  and  $\text{GR2}_{\text{ab+cells}}/\text{MR}$ , Fig. 5). These stabilizing  
487 compounds have already proved their ability to prevent the formation of magnetite from  
488  $\text{GR1}_{\text{ab}}$  or  $\text{GR1}_{\text{bio}}$  dissolution (Bocher *et al.*, 2004; Jorand *et al.*, 2013). It was suggested that  
489 reactive ferrous sites involved in GR dissolution and located on the lateral faces would be  
490 hidden by phosphate (Bocher *et al.*, 2004). For example, the reduction of nitrate by  $\text{GR1}$   
491 implies these lateral  $\text{Fe}^{\text{II}}$  sites, and its kinetics is strongly affected by phosphate (Etique *et al.*,  
492 2014b), by EPS (Zegeye *et al.*, 2014), or by silicate (data not shown). In the present

493 investigation, since GR stabilizing agents affect MR reduction, MR would preferentially react  
494 with the same  $\text{Fe}^{\text{II}}$  sites of GR as those involved by the sorbing ligands. As  $\text{Hg}^{\text{II}}$  reduction was  
495 slightly affected by phosphate or cells, we may suppose that  $\text{Hg}^{\text{II}}$  would preferentially react  
496 with other reactive sites, which might rather be located on the basal face of the GR crystal.  
497 Other GR stabilizers such as silicate and paa, are also known to prevent unstable GRs from  
498 transforming into magnetite (Sergent *et al.*, 2011; Jorand *et al.*, 2013), however, they affect to  
499 a lesser degree the MR reduction by GRs.

500 In addition, the presence of sorbing ligands could slow down the reactivity of GRs by  
501 electrostatic repulsion and/or steric hindrance. Indeed, the interactions of negatively charged  
502 MR with GR surfaces covered with a layer of anionic ligands such as phosphate anions, cells,  
503 or polymers might also explain the decrease in the reduction rate of MR as compared to that  
504 of Hg.

## 505 **5. Conclusion**

506 The difference in reactivity between GRs has more to do with the nature of the  
507 contaminant ( $\text{Hg}^{\text{II}}$  or MR) than with the type of GRs (GR1 or GR2). At pH 7, the reaction of  
508 GRs with MR is generally slower than with  $\text{Hg}^{\text{II}}$ , and moreover, the reduction of MR seems to  
509 be more affected by stabilizing agents than  $\text{Hg}^{\text{II}}$  reduction. More precisely, the reduction of  
510 MR is sharply limited by phosphate and bacterial cells, whereas in the presence of silicate and  
511 paa this reduction is moderate. This difference in GR reactivity towards mercury and methyl  
512 red would probably be based on the nature of  $\text{Fe}^{\text{II}}$  surface sites involved during the reduction:  
513 lateral  $\text{Fe}^{\text{II}}$  surface sites would be monopolized for MR reduction, whereas basal  $\text{Fe}^{\text{II}}$  surface  
514 sites would interact with  $\text{Hg}^{\text{II}}$  species.

515 Although the  $\text{Hg}^{\text{II}}$  reduction is slightly hindered in the presence of stabilizing agents, the  
516 variation of pH suspension from 7.0 to 9.5 leads to a decrease of the kinetics rate. This  
517 finding can be explained by the fluctuation of the surface charge of GR (pH 7.0: positive, pH

518 8.2: zero, pH 9.5: negative) that governs the adsorption and the reduction of  $\text{Hg}(\text{OH})_2$ , the  
519 predominant phase of  $\text{Hg}^{\text{II}}$  species at pH of this investigation.

520 In environmental conditions where the fougèrite mineral can be represented by  
521 biologically synthesized hydroxycarbonate green rust ( $\text{GR1}_{\text{bio}}$ ),  $\text{Hg}^{\text{II}}$  species would be more  
522 reduced than MR. Indeed, the amount of  $\text{Hg}^{\text{II}}$  species reduced by surface area of  $\text{GR1}_{\text{bio}}$   
523 ( $1.1 \times 10^{-4}$  moles of  $\text{Hg}^{\text{II}} \text{ m}^{-2}$ ) is significantly higher than those of MR ( $4.3 \times 10^{-6}$  moles of  
524  $\text{MR m}^{-2}$ ). In engineering applications using GRs as a reactive sorbent and/or reducing agent,  
525 more attention should be paid to the co-occurring ligands as regards the type of target  
526 pollutants. These results have strong implications in attenuation and remediation studies  
527 aiming to predict the fate and transport of methyl red and mercury in natural or engineered  
528 systems.

## 529 **Acknowledgements**

530 The authors acknowledge financial support from the Agence Nationale de la Recherche  
531 (France) (“Arctic Metals” project), the Ministère de l’Enseignement Supérieur et de la  
532 Recherche (France), and the Zone Atelier Moselle (Lorraine, France). We thank J. Ghanbaja  
533 for TEM analysis, I. Bihannic for XRD analysis, B. Grégoire and A. Razafitianamaharavo for  
534 BET analysis, and M. Abdelmoula for TMS analysis.

535

## 536 **List of symbols**

- 537  $\text{GR1}_{\text{ab}}$ : abiotically synthesized hydroxycarbonate green rust  
538  $\text{GR2}_{\text{ab}}$ : abiotically synthesized hydroxysulfate green rust  
539  $\text{GR1}_{\text{bio}}$ : microbially synthesized hydroxycarbonate green rust  
540  $\text{GR1}_{\text{ab+P}}$ : abiotically synthesized hydroxycarbonate green rust with phosphate  
541  $\text{GR1}_{\text{ab+Si}}$ : abiotically synthesized hydroxycarbonate green rust with silicic acid  
542  $\text{GR1}_{\text{ab+paa}}$ : abiotically synthesized hydroxycarbonate green rust with polyacrylic acid



543	GR <sub>2ab+cells</sub> :	abiotically synthesized hydroxysulfate green rust with heat-killed cells
544	A:	surface area concentration ( $\text{m}^2 \text{L}^{-1}$ )
545	$k_{\text{obs}}$ :	pseudo first-order rate constant ( $\text{min}^{-1}$ )
546	$k_{\text{FeII}}$ :	$k_{\text{obs}}$ normalized to the $\text{Fe}^{\text{II}}$ content of GRs ( $\text{L mmol}^{-1} \text{min}^{-1}$ )
547	$k_{\text{s}}$ :	$k_{\text{obs}}$ normalized to the estimated $\text{Fe}^{\text{II}}$ surface sites of GRs ( $\text{L mmol}^{-1} \text{min}^{-1}$ )
548	paa:	polyacrylic acid

549

## 550 **Appendix A. Supplementary data**

551 Supplementary data associated with this article (Tables S1 – S4; Notes S1 – S3; and Fig. S1 –  
552 S6) can be downloaded online.

553

## 554 **References**

- 555 Bearcock, J. M., Perkins, W. T., Pearce, N. J. G., 2011. Laboratory studies using naturally  
556 occurring "green rust" to aid metal mine water remediation. *Journal of Hazardous*  
557 *Materials* 190, 466–473.
- 558 Benali, O., Abdelmoula, M., Refait, P., Génin, J.-M. R. 2001. Effect of orthophosphate on the  
559 oxidation products of Fe(II)–Fe(III) hydroxycarbonate: the transformation of green rust to  
560 ferrihydrite. *Geochimica et Cosmochimica Acta* 65, 1715–1726.
- 561 Bocher, F., Géhin, A., Ruby, C., Ghanbaja, J., Abdelmoula, M., Génin J.-M. R. 2004.  
562 Coprecipitation of Fe(II–III) hydroxycarbonate green rust stabilized by phosphate  
563 adsorption. *Solid State Sciences* 6 (1), 117–124.
- 564 Carlson, H. K., Clark, I. C., Melnyk, R. A., Coates, J. D. 2012. Toward a mechanistic  
565 understanding of anaerobic nitrate-dependent iron oxidation: balancing electron uptake and  
566 detoxification. *Frontiers in Microbiology* 3 (57), 1–6.

- 567 Charlet, L., Bosbach, D., Peretyashko, T. 2002. Natural attenuation of TCE, As, Hg linked to  
568 the heterogeneous oxidation of Fe(II): an AFM study. *Chemical Geology* 190, 303–319.
- 569 Christiansen, B. C., Balic-Zunic, T., Dideriksen, K., Stipp, S. L. S. 2009. Identification of  
570 green rust in groundwater. *Environmental Science & Technology* 43, 3436–3441.
- 571 Drissi, S. H., Refait, P., Abdelmoula, M., Génin, J.-M. R. 1995. The preparation and  
572 thermodynamic properties of iron(II)-iron(III) hydroxide-carbonate (green rust); Pourbaix  
573 diagram of iron in carbonate-containing aqueous media. *Corrosion Science* 37, 2025–2041.
- 574 Elsner M., Schwarzenbach R. P., Haderlein, S. B. 2004. Reactivity of Fe(II)-bearing minerals  
575 toward reductive transformation of organic contaminants. *Environmental Science &*  
576 *Technology* 38, 799–807.
- 577 Erbs, M., Hansen, H. S. B., Olsen, C. E. 1999. Reductive dechlorination of carbon  
578 tetrachloride using iron(II) iron(III) hydroxide sulfate (green rust). *Environmental Science*  
579 *& Technology* 33, 307–311.
- 580 Etique, M., Jorand, F. P. A., Zegeye, A., Grégoire, B., Despas, C., Ruby, C. 2014a. Abiotic  
581 process for Fe(II) oxidation and green rust mineralization driven by a heterotrophic nitrate  
582 reducing bacteria (*Klebsiella mobilis*). *Environmental Science & Technology* 48,  
583 3742–3751.
- 584 Etique, M., Zegeye, A., Grégoire, B., Carteret, C., Ruby, C. 2014b. Nitrate reduction by  
585 mixed iron(II-III) hydroxycarbonate green rust in the presence of phosphate anions: the  
586 key parameters influencing the ammonium selectivity. *Water Research* 62, 29–39.
- 587 Fredrickson, J. K., Zachara, J. M., Kennedy, D. W., Dong, H., Onstott, T. C., Hinman, N. W.,  
588 Li, S.-M. 1998. Biogenic iron mineralization accompanying the dissimilatory reduction of  
589 hydrous ferric oxide by a groundwater bacterium. *Geochimica et Cosmochimica Acta* 62,  
590 3239–3257.

- 591 Génin, J.-M. R., Abdelmoula, M., Ruby, C., Upadhyay, C. 2006. Speciation of iron;  
592 characterisation and structure of green rusts and Fe<sup>II-III</sup> oxyhydroxycarbonate fougérite.  
593 Comptes Rendus Geosciences 338, 402-419.
- 594 Génin, J.-M. R., Bourrié, G., Trolard, F., Abdelmoula, M., Jaffrezic, A., Refait, P., Maître, V.,  
595 Humbert, B., Herbillon, A. 1998. Thermodynamic equilibria in aqueous suspensions of  
596 synthetic and natural Fe(II)–Fe(III) green rusts: occurrences of the mineral in  
597 hydromorphic soils. Environmental Science & Technology 32, 1058–1068.
- 598 Guilbaud, R., White, M. L., Poulton, S. W. 2013. Surface charge and growth of sulphate and  
599 carbonate green rust in aqueous media. Geochimica et Cosmochimica Acta 108, 141-153.
- 600 Hansen, H. C. B., Guldborg, S., Erbs, M., Koch, C.-B. 2001. Kinetics of nitrate reduction by  
601 green rusts effects of interlayer anion and Fe(II):Fe(III) ratio. Applied Clay Sciences 18,  
602 81–91.
- 603 Hou, X.-L., Yang, Z., Yeung, K.-S., Wong, H. N. C., 2007. Chapter 5.3 Five-membered ring  
604 systems: furans and benzofurans. Progress in Heterocyclic Chemistry 18, (C), 187–217.
- 605 Jorand, F. P. A, Sergent, A.-S., Remy, P.-P., Bihannic, I., Ghanbaja, J., Lartiges, B., Hanna,  
606 K., Zegeye, A. 2013. Contribution of anionic vs neutral polymers to the formation of green  
607 rust 1 from  $\gamma$ -FeOOH bioreduction. Geomicrobiology Journal 30, 600–615.
- 608 Khalid, A., Arshad, M., Crowley, D. E. 2008. Decolorization of azo dyes by *Shewanella* sp.  
609 under saline conditions. Applied Microbiology and Biotechnology 79, 1053-1059.
- 610 Kone, T., Hanna, K., Abdelmoula, M., Ruby, C., Carteret, C., 2009. Reductive transformation  
611 and mineralization of an azo dye by hydroxysulphate green rust preceding oxidation using  
612 H<sub>2</sub>O<sub>2</sub> at neutral pH. Chemosphere 75, 212–219.
- 613 Lee, W., Batchelor, B., 2002. Abiotic reductive dechlorination of chlorinated ethylenes by  
614 iron-bearing soil minerals. 2. Green rust. Environmental Science & Technology 36, 5348-  
615 5354.

- 616 Loyaux-Lawniczak, S., Refait, P., Ehrhardt, J.-J., Lecomte, P., Génin, J.-M. R., 2000.  
617 Trapping of Cr by formation of ferrihydrite during the reduction of chromate ions by  
618 Fe(II)-Fe(III) hydroxysalt green rusts. *Environmental Science & Technology* 34, 438-443.
- 619 Mills, S. J., Christy, A. G., Génin, J.-M. R., Kameda, T., Colombo, F., 2012. Nomenclature of  
620 the hydrotalcite supergroup: natural layered double hydroxides. *Mineralogical Magazine*  
621 76, 1289-1336.
- 622 Mishra, B., O'Loughlin, E. J., Boyanov, M. I., Kemner, K. M., 2011. Binding of Hg<sup>II</sup> to high-  
623 affinity sites on bacteria inhibits reduction to Hg<sup>0</sup> by Mixed Fe<sup>II/III</sup> phases. *Environmental*  
624 *Science & Technology* 45, 9597–9603.
- 625 Mitsunobu, S., Takahashi, Y., Sakai, Y., 2008. Abiotic reduction of antimony (V) by green  
626 rust (Fe<sub>4</sub>(II)Fe<sub>2</sub>(III)(OH)<sub>12</sub>SO<sub>4</sub> · 3H<sub>2</sub>O). *Chemosphere* 70, 942–947.
- 627 Myneni, S. C. B., Tokunaga, T. K., Brown Jr., G. E., 1997. Abiotic Se redox chemistry in the  
628 presence of Fe(II, III)-oxides. *Science* 278, 1106 – 1109.
- 629 O'Loughlin, E. J., Burriss, D. R., 2004. Reduction of halogenated ethanes by green rust.  
630 *Environmental Toxicology and Chemistry* 23, 41-48.
- 631 O'Loughlin, E. J., Kelly, S. D., Kemner, K. M., Csencsits R., Cook, R. E. 2003. Reduction of  
632 Ag<sup>I</sup>, Au<sup>III</sup>, Cu<sup>II</sup>, and Hg<sup>II</sup> by Fe<sup>II</sup>/Fe<sup>III</sup> hydroxysulfate green rust. *Chemosphere* 53, 437-446.
- 633 O'Loughlin, E. J., Gorski C. A., Scherer M. M., Boyanov M. J., Kemner K. M. 2010. Effects  
634 of oxyanions, natural organic matter, and bacterial cell numbers on the bioreduction of  
635 lepidocrocite ( $\gamma$ -FeOOH) and the formation of secondary mineralization products.  
636 *Environmental Science & Technology* 44, 4570-4576.
- 637 Ona-Nguema, G., Abdelmoula, M., Jorand, F., Benali, O., Géhin, A., Block, J.-C., Génin J.-M.  
638 R., 2002. Iron (II, III) hydroxycarbonate green rust formation and stabilization from  
639 lepidocrocite bioreduction. *Environmental Science & Technology* 36, 16-20.

- 640 Pasakarnis, T. S., Boyanov, M. I., Kemner, K. M., Mishra, B., O'Loughlin, E. J., Parkin, G.,  
641 Scherer, M. M., 2013. Influence of chloride and Fe(II) content on the reduction of Hg(II)  
642 by magnetite. *Environmental Science & Technology* 47, 6987-6994.
- 643 Pourbaix, M., 1963. Atlas d'équilibres électrochimiques. Gauthier-Villars et Cie, Paris, pp.  
644 422-427.
- 645 Refait, P., Memet, J.-B., Bon, C., Sabot, R., Génin, J.-M. R., 2003. Formation of the Fe(II)–  
646 Fe(III) hydroxysulphate green rust during marine corrosion of steel. *Corrosion Science* 45,  
647 833-845.
- 648 Refait, P., Abdelmoula, M., Génin, J.-M. R., Sabot, R., 2006. Green rusts in electrochemical  
649 and microbially influenced corrosion of steel. *Comptes Rendus Geosciences* 338, 476-487.
- 650 Ruby, C., Géhin, A., Abdelmoula, M., Génin, J.-M. R., Jolivet, J. P., 2003. Coprecipitation of  
651 Fe(II) and Fe(III) cations in sulphated aqueous medium and formation of hydroxysulphate  
652 green rust. *Solid State Sciences* 5, 1055-1062.
- 653 Ruby, C., Haissa, R., Géhin, A., Abdelmoula, M., Génin, J.-M. R., 2006. Chemical stability  
654 of hydroxysulphate green rust synthesized in the presence of foreign anions: carbonate,  
655 phosphate and silicate. *Hyperfine Interactions* 167, 803-807.
- 656 Schwertmann, U., Fechter, H., 1994. The formation of green rust and its transformation to  
657 lepidocrocite. *Clay Minerals* 29, 87-92.
- 658 Sergent, A.-S., Jorand, F., Hanna, K., 2011. Effects of Si-bearing minerals on the nature of  
659 secondary iron mineral products from lepidocrocite bioreduction. *Chemical Geology* 289,  
660 86–97.
- 661 Simon L., Francois M., Refait P., Renaudin G., Lelaurain M., and Génin J.-M. R., 2003.  
662 Structure of the Fe(II-III) layered double hydroxysulphate green rust two from Rietveld  
663 analysis. *Solid State Sciences* 5, 327–334.

- 664 Su, C, Puls, R. W., 2004. Significance of iron(II,III) hydroxycarbonate green rust in arsenic  
665 remediation using zerovalent iron in laboratory column tests. *Environmental Science &*  
666 *Technology* 38, 5224-5231.
- 667 Taylor, R. M., Schwertmann, U., Fechter, H., 1985. A rapid method for the formation of  
668 Fe(II)-Fe(III) hydroxycarbonate. *Clay Minerals* 20, 147–151.
- 669 Viollier, E., Inglett, P. W., Hunter, K., Roychoudhury, A. N., Van Cappellen, P. 2000. The  
670 ferrozine method revisited: Fe(II)/Fe(III) determination in natural waters. *Applied*  
671 *Geochemistry* 15, 785-790.
- 672 Wiatrowski, H. A., Das, S., Kukkadapu, R., Ilton, E. S., Barkay, T., Yee, N. 2009. Reduction  
673 of Hg(II) to Hg(0) by magnetite. *Environmental Science & Technology* 43, 5307–5313.
- 674 Wiatrowski, H. A., Ward, P. M., Barkay, T., 2006. Novel reduction of mercury(II) by  
675 mercury-sensitive dissimilatory metal reducing bacteria. *Environmental Science &*  
676 *Technology* 40, 6690–6696.
- 677 Williams, A., Scherer, M. M., 2001. Kinetics of Cr(VI) reduction by carbonate green rust.  
678 *Environmental Science & Technology* 35, 3488–3494.
- 679 Zegeye, A., Bonneville, S., Benning, L. G., Sturm A., Fowle D. A., Jones, C. A., Canfield, D.  
680 E., Ruby C., MacLean, L. C., Nomosatryo, S., Crowe, S. A., Poulton, S. W., 2012. Green  
681 rust formation controls nutrient availability in a ferruginous water column. *Geology* 40,  
682 599-602.
- 683 Zegeye, A., Etique, M., Carteret, C., Ruby, C., Schaaf, P., Francius, G., 2014 Origin of the  
684 differential nanoscale reactivity of biologically and chemically formed green rusts crystals  
685 investigated by chemical force spectroscopy. *Journal of Physical Chemistry C* 118, 5978–  
686 5987.
- 687 Zegeye, A., Mustin, C., Jorand, F. 2010. Bacterial and iron oxide aggregates mediate  
688 secondary iron mineral formation: green-rust vs magnetite. *Geobiology* 8, 209-22.

- 689 Zegeye, A., Ona-Nguema, G., Carteret, C., Huguet, L., Abdelmoula, M., Jorand, F., 2005.  
690 Formation of hydroxysulphate green rust 2 as a single iron(II–III) mineral in microbial  
691 culture. *Geomicrobiology Journal* 22, 389–399.
- 692 Zegeye, A., Ruby, C., Jorand, F., 2007. Kinetic and thermodynamic analysis during  
693 dissimilatory  $\gamma$ -FeOOH reduction: formation of green rust 1 and magnetite.  
694 *Geomicrobiology Journal* 24, 51-64.

ACCEPTED MANUSCRIPT

1 Table 1. Kinetics rate constants ( $k_{\text{obs}}$ ,  $\text{min}^{-1}$ ),  $k_{\text{obs}}$  normalized to surface  $\text{Fe}^{\text{II}}$  sites ( $k_{\text{s}}$ ,  $\text{L mmol}^{-1} \text{min}^{-1}$ ) and  $k_{\text{obs}}$  normalized to structural  $\text{Fe}^{\text{II}}$  ( $k_{\text{Fe}^{\text{II}}}$ ,  $\text{L mmol}^{-1} \text{min}^{-1}$ ) of the reduction of  $\text{Hg}^{\text{II}}$  ( $5 \mu\text{M}$ ) by chemically synthesized carbonated green rust (GR1<sub>ab</sub> or GR1<sub>ab+P</sub> supplemented with phosphate),  
 2 biogenic carbonated green rust (GR1<sub>bio</sub>), chemically synthesized sulfated green rust (GR2<sub>ab</sub>), or GR2<sub>ab</sub> with a cell suspension (GR2<sub>ab+cells</sub>). Each  
 3 batch was conducted with 0.5 mM ( $\text{Hg}^{\text{II}}/\text{GR} = 1/100$ ) or 0.05 mM ( $\text{Hg}^{\text{II}}/\text{GR} = 1/10$ ) of GR in duplicates (except when specified). A = surface  
 4 area concentration ( $\text{m}^2 \text{L}^{-1}$ ). ND = not determined.

	A	Structural $\text{Fe}^{\text{II}}$ (mM)	Surface $\text{Fe}^{\text{II}}$ sites ( $\mu\text{M}$ )	$\text{Hg}^{\text{II}}/\text{GR}$	Rate constants	pH 7.0 $\times 10^{-2}$	pH 8.2 $\times 10^{-2}$	pH 9.5 $\times 10^{-2}$
GR1 <sub>ab</sub>	$10 \pm 2^a$	2.2	83	1/100	$k_{\text{obs}}$ $k_{\text{s}}^{\text{II}}$ $k_{\text{Fe}^{\text{II}}}$	ND ND ND	$2.5 \pm 0.3$ $30 \pm 3$ $1.1 \pm 0.1$	ND ND ND
		0.22	8.3	1/10	$k_{\text{obs}}$ $k_{\text{s}}^{\text{II}}$ $k_{\text{Fe}^{\text{II}}}$	ND ND ND	$8.6 \pm 0.1$ $1036 \pm 12$ $39.1 \pm 0.5$	ND ND ND
GR1 <sub>ab+P</sub>	$10 \pm 2$	1.2	83	1/100	$k_{\text{obs}}$ $k_{\text{s}}^{\text{II}}$ $k_{\text{Fe}^{\text{II}}}$	$3.8 \pm 0.2$ $45 \pm 2$ $3.2 \pm 0.2$	$3.0 \pm 0.6$ $36 \pm 7$ $2.5 \pm 0.5$	$3.1 \pm 0.2$ $37 \pm 2$ $2.6 \pm 0.2$
GR1 <sub>bio</sub>	4.2	1.3	34.8	1/80	$k_{\text{obs}}$ $k_{\text{s}}^{\text{II}}$ $k_{\text{Fe}^{\text{II}}}$	$4.1 \pm 0.2$ $118 \pm 6$ $3.1 \pm 0.1$	$2.2 \pm 0.3$ $63 \pm 8$ $1.7 \pm 0.2$	$2.7 \pm 0.5$ $78 \pm 14$ $2.1 \pm 0.4$
		0.13	3.48	1/8	$k_{\text{obs}}$ $k_{\text{s}}^{\text{II}}$ $k_{\text{Fe}^{\text{II}}}$	ND ND ND	$3.5 \pm 0.4$ $1006 \pm 114$ $27 \pm 3$	ND ND ND
		0.013	0.348	1/0.8	$k_{\text{obs}}$ $k_{\text{s}}^{\text{II}}$ $k_{\text{Fe}^{\text{II}}}$	ND ND ND	$1.5^b$ $4310$ $115$	ND ND ND
GR2 <sub>ab</sub>	$4.6 \pm 0.7$	2.0	38.2	1/100	$k_{\text{obs}}$ $k_{\text{s}}^{\text{II}}$ $k_{\text{Fe}^{\text{II}}}$	$4.1 \pm 0.2$ $107 \pm 5$ $2.0 \pm 0.1$	$1.6 \pm 0.1$ $42 \pm 2$ $0.80 \pm 0.05$	$1.1^b$ 29 0.6
GR2 <sub>ab+cells</sub>	$4.6 \pm 0.7$	2.0	38.2	1/100	$k_{\text{obs}}$ $k_{\text{s}}$ $k_{\text{Fe}^{\text{II}}}$	$1.8 \pm 0.4^c$ $47 \pm 11$ $0.9 \pm 0.2$	$2.1 \pm 0.5$ $55 \pm 13$ $1.05 \pm 0.25$	$2.8 \pm 0.9$ $73 \pm 24$ $1.4 \pm 0.5$

6 <sup>a</sup> Assuming the surface area was the same than GR1<sub>ab+P</sub>

7 <sup>b</sup>  $n = 1$

8 <sup>c</sup>  $n = 3$  independent experiments



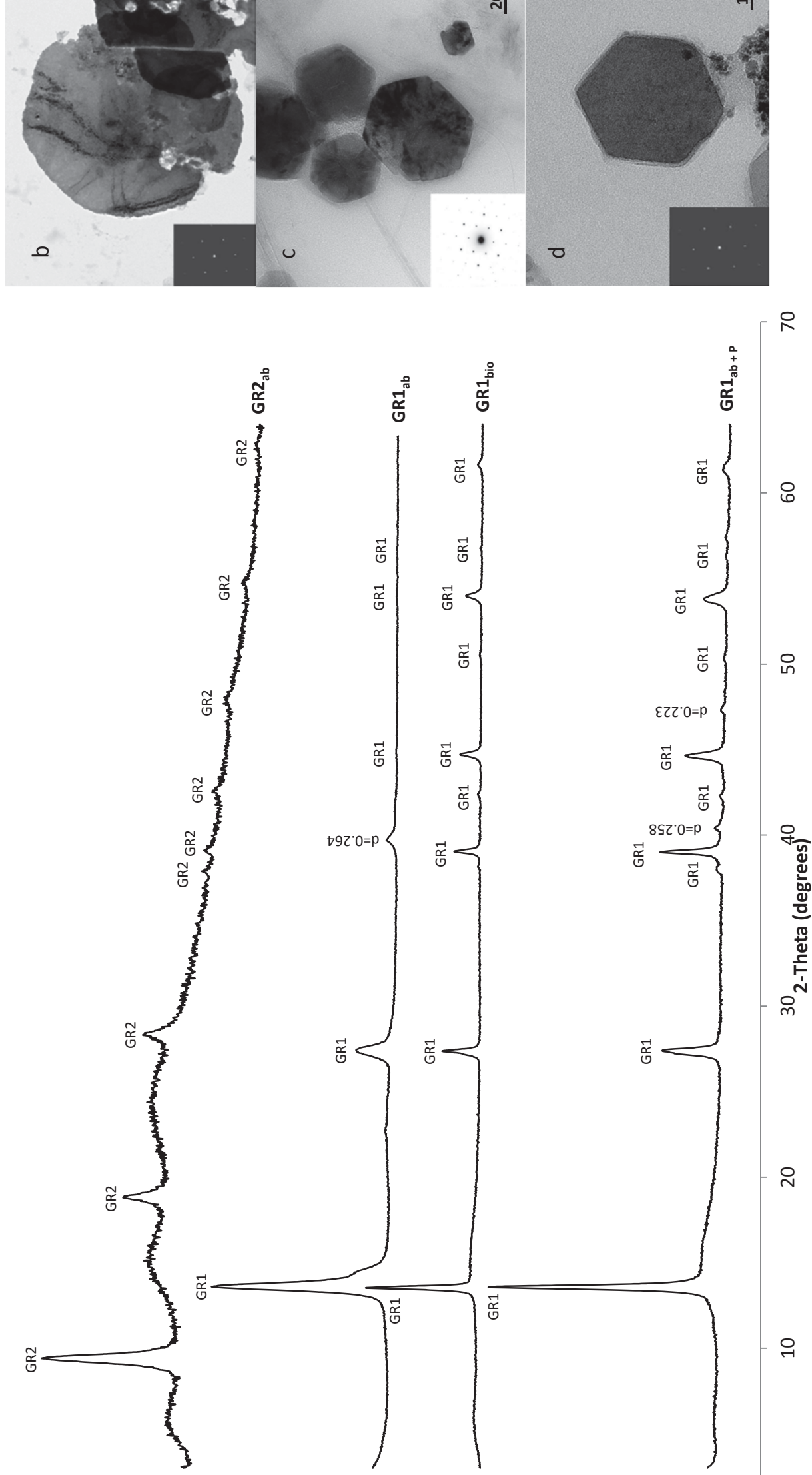
9 Table 2: Kinetics rate constants ( $k_{\text{obs}}$ ),  $k_{\text{obs}}$  normalized to surface  $\text{Fe}^{\text{II}}$  ( $k_s$ ,  $\text{L mmol}^{-1} \text{min}^{-1}$ ) and  $k_{\text{obs}}$  normalized to structural  $\text{Fe}^{\text{II}}$  ( $k_{\text{Fe}}$ ,  $\text{L mmol}^{-1}$   
 10  $\text{min}^{-1}$ ) of the reduction of methyl red (MR) by chemically synthesized carbonated green rust (GR<sub>1-ab</sub>), GR<sub>1-ab</sub> supplemented with 4 mM phosphate  
 11 (GR<sub>1-ab+p</sub>) or with 4 mM  $\text{H}_4\text{SiO}_4$  (GR<sub>1-ab+Si</sub>) or with 0.5  $\text{g L}^{-1}$  of polyacrylic acid (GR<sub>1-ab+paa</sub>) or by biogenic carbonated green rust (GR<sub>1-bio</sub>),  
 12 chemically synthesized sulfated green rust (GR<sub>2-ab</sub>), or GR<sub>2-ab</sub> supplemented with a cell suspension (GR<sub>2-ab+cells</sub>). All experiments were done at pH  
 13  $7.0 \pm 0.1$  and in duplicates (except for GR<sub>1-ab+Si</sub>). A = surface area concentration.

	A	Structural $\text{Fe}^{\text{II}}$ (mM)	Surface $\text{Fe}^{\text{II}}$ sites ( $\mu\text{M}$ )	MR/GR	$k_{\text{obs}} \times 10^{-3}$ ( $\text{min}^{-1}$ )	$k_s \times 10^{-3}$ ( $\text{L mmol}^{-1} \text{min}^{-1}$ )	$k_{\text{Fe}} \times 10^{-3}$ ( $\text{L mmol}^{-1} \text{min}^{-1}$ )
GR <sub>1-ab</sub>	$10 \pm 2^a$	2.2	83	1/33	$28 \pm 4$	$337 \pm 48$	$13 \pm 2$
GR <sub>1-ab+p</sub>	$10 \pm 2$	1.2	83	1/33	$0.6 \pm 0.1$	$7 \pm 1$	$0.5 \pm 0.1$
GR <sub>1-ab+Si</sub>	$10 \pm 2^a$	1.2	83	1/33	$13^b$	156	11
GR <sub>1-ab+paa</sub>	$10 \pm 2^a$	1.2	83	1/33	$16^b$	193	13
GR <sub>1-bio</sub>	4.2	1.3	34.8	1/26	$2.0 \pm 0.2$	$57 \pm 6$	$1.5 \pm 0.1$
GR <sub>2-ab</sub>	$4.6 \pm 0.7$	2.0	38.2	1/33	$130 \pm 50$	$3403 \pm 1308$	$65 \pm 25$
GR <sub>2-ab+cells</sub>	$4.6 \pm 0.7$	2.0	38.2	1/33	$0.6 \pm 0.2$	$16 \pm 5$	$0.3 \pm 0.1$

14 <sup>a</sup> Assuming the surface area was the same than GR<sub>1-ab+p</sub>

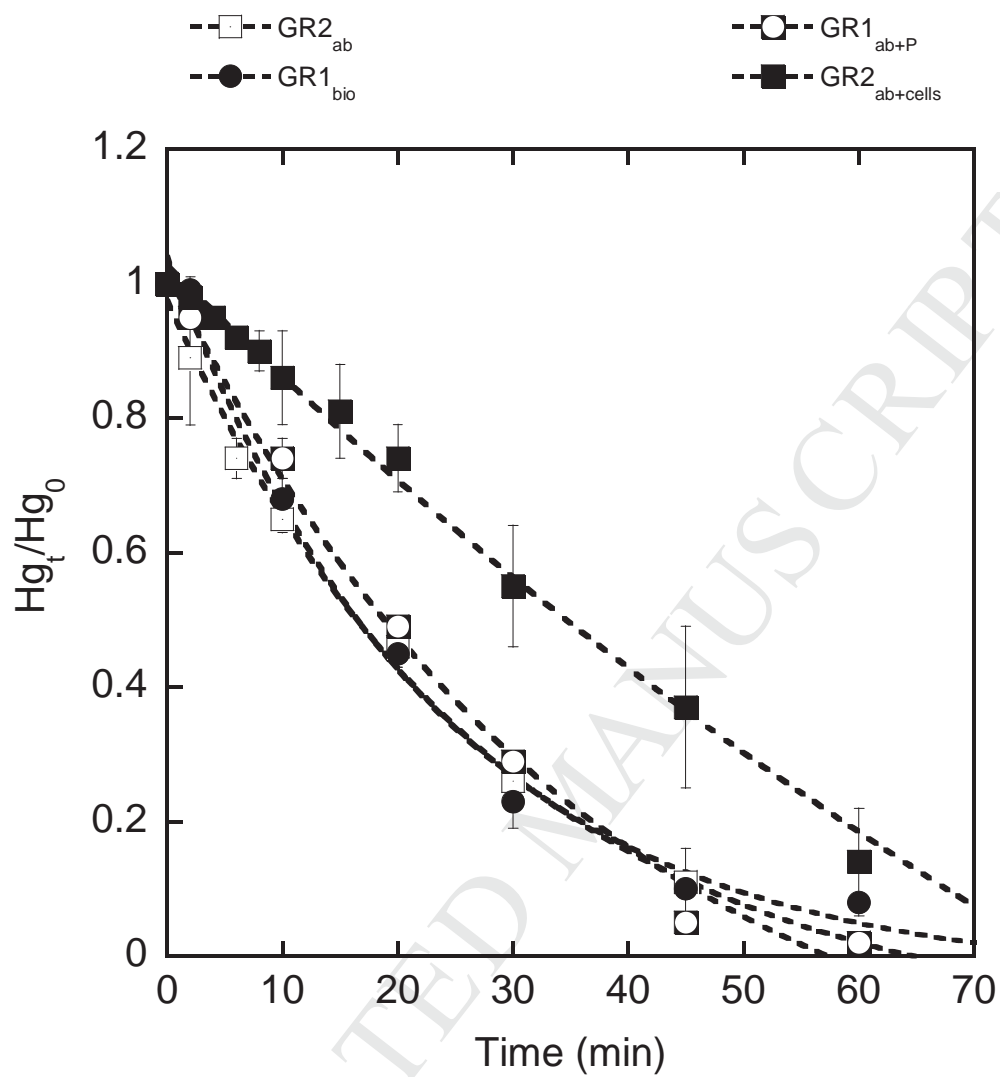
15 <sup>b</sup>  $n = 1$

16



**Fig. 1.** X-ray diffractograms (Co,  $l = 0.178897$  nm) of the biogenic carbonated green rust 1 after microbial reduction of lepidocrocite ( $\gamma$ -FeOOH) by *Shewanella putrefaciens* (GR1<sub>bio</sub>), chemically synthesized carbonated green rust 1 (GR1<sub>ab</sub>), chemically synthesized carbonated green rust 1 stabilized by phosphate (GR1<sub>ab+P</sub>) and sulfated green rust 2 (GR2<sub>ab</sub>) (a); images of GR1<sub>bio</sub> (b), GR2<sub>ab</sub> (c), and GR1<sub>ab+P</sub> (d) crystals. Inserts show the electron diffraction pattern of each GR. With GR1<sub>ab+P</sub> a few minor peaks ( $d = 0.186$  nm;  $d = 0.223$  nm;  $d = 0.258$  nm) were detected on XRD diffractogram (a), corresponding probably to chukanovite ( $\text{Fe}_2(\text{OH})_2\text{CO}_3$ ), but this phase was not confirmed by Mössbauer analysis.

a)

1  
2

3

4

5

6

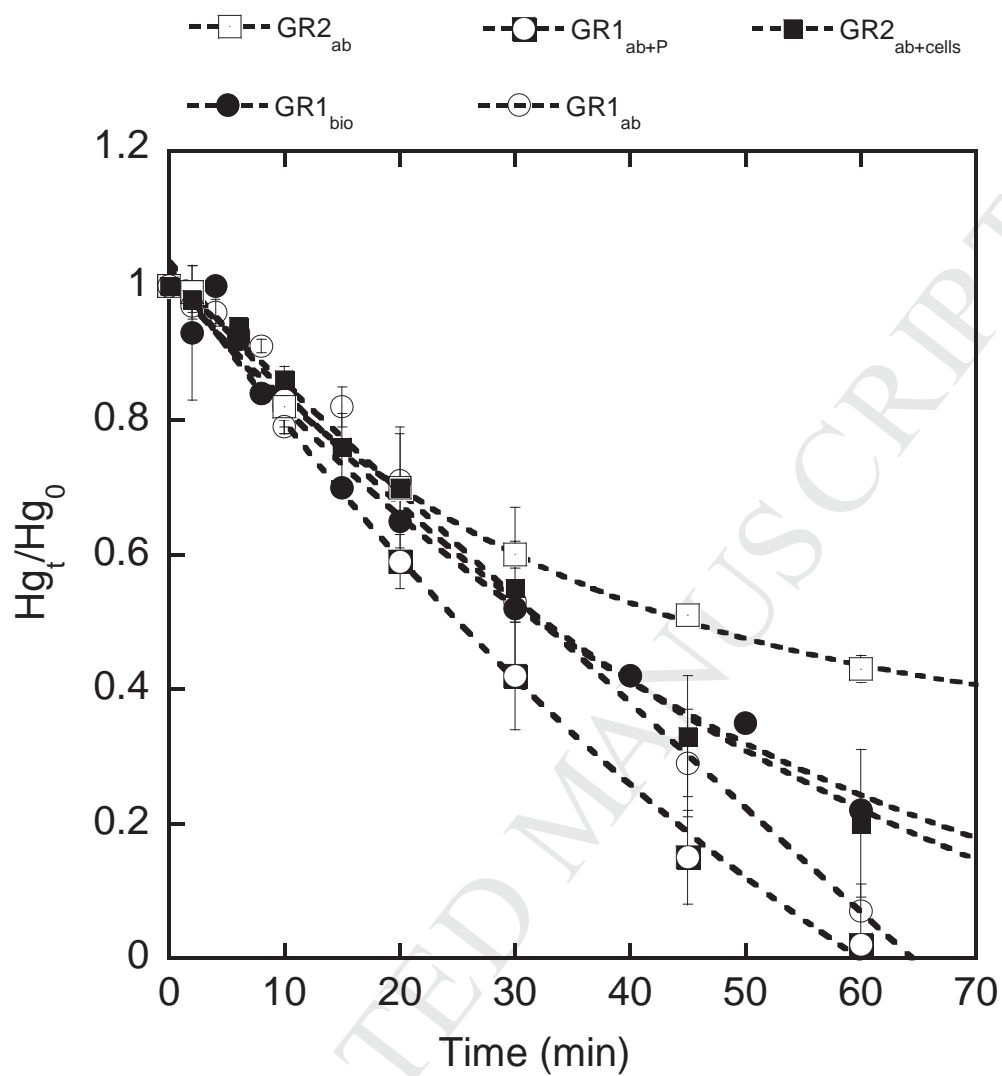
7

8

9

10 Fig 2a

b)

11  
12

13

14

15

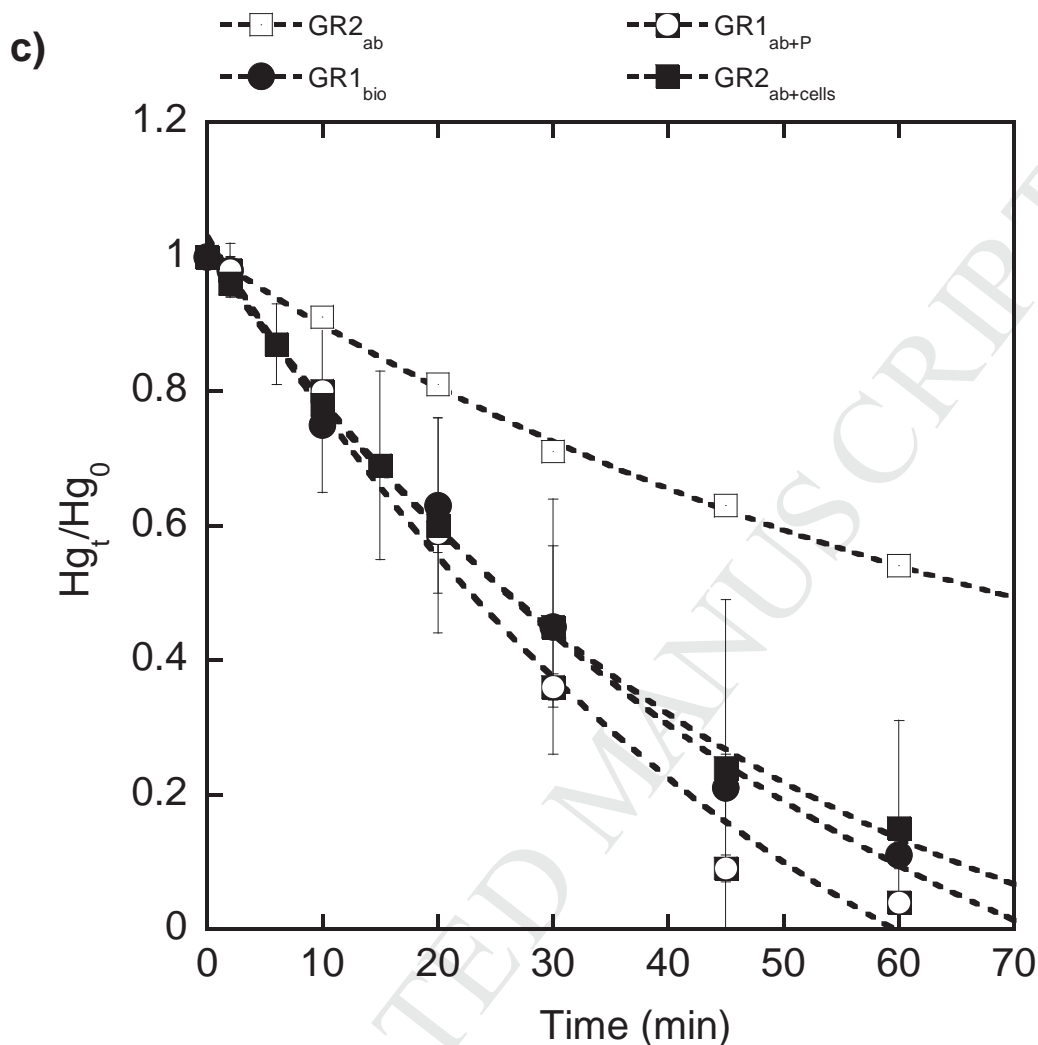
16

17

18

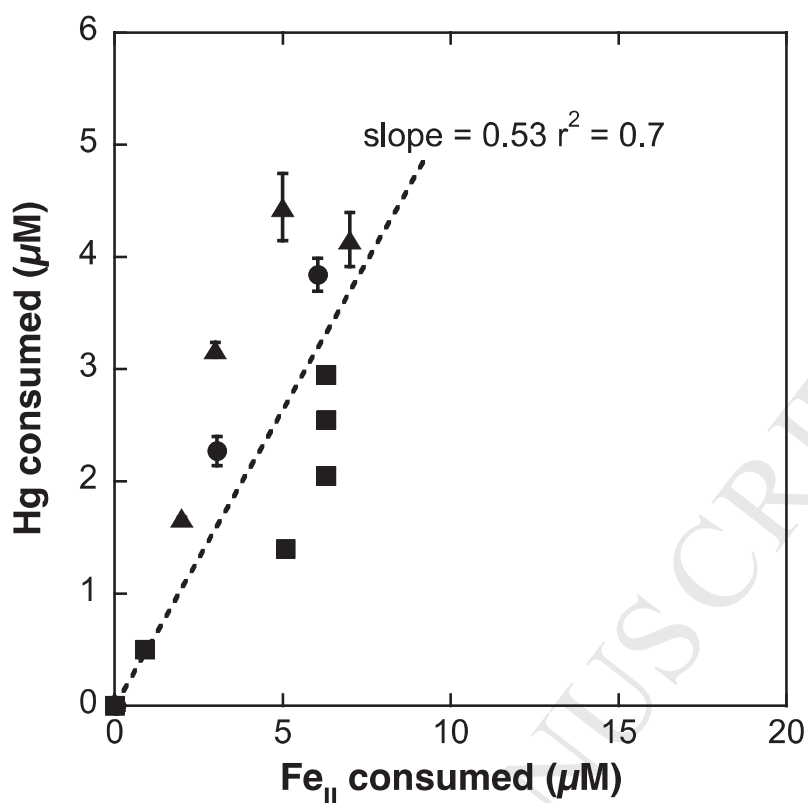
19

20 Fig 2b



21  
22

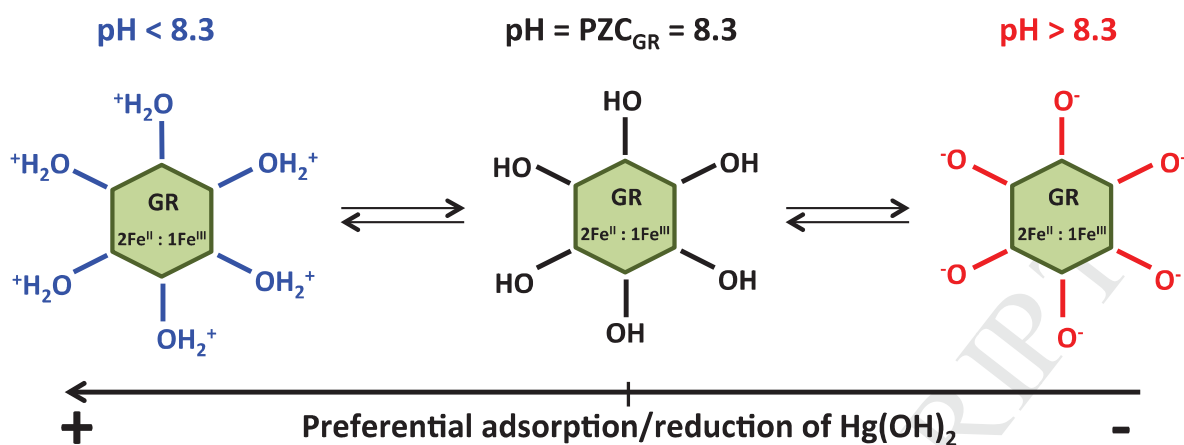
23 **Fig. 2.** Removal of mercury over time in the presence of green rusts: 400  $\mu\text{M}$  of biologically  
 24 synthesized hydroxycarbonate green rust ( $\text{GR1}_{\text{bio}}$ ), and 500  $\mu\text{M}$  of chemically synthesized  
 25 hydroxycarbonate green rust ( $\text{GR1}_{\text{ab}}$ ),  $\text{GR1}_{\text{ab}}$  supplemented with phosphate ( $\text{GR1}_{\text{ab+P}}$ ),  
 26 hydroxysulfate green rust ( $\text{GR2}_{\text{ab}}$ ) and  $\text{GR2}_{\text{ab}}$  supplemented with cells ( $\text{GR2}_{\text{ab+cells}}$ ). The  
 27 amount of Hg remaining in solution ( $\text{Hg}_t/\text{Hg}_0$ ) is plotted as a function of time at a pH of  
 28  $7.0 \pm 0.1$  (a),  $8.2 \pm 0.1$  (b), and  $9.5 \pm 0.1$  (c). The changes in pH after a 60 h incubation time  
 29 period are reported in Table S7. Bars are the errors of two independent experiments.



1  
2  
3  
4  
5  
6  
7

**Fig. 3.** Evolution of the mercury consumption as a function of the Fe<sup>II</sup> consumption for time between 0 and 60 min with Hg<sup>II</sup>/GR ratios of 1/10 for GR1<sub>ab</sub> (circle), 1/8 (triangle) and 1/0.8 (square) for GR1<sub>bio</sub>. The slope of 0.53 fits well with the expected ratio Hg<sup>II</sup>:Fe<sup>II</sup><sub>GR</sub> of 1:2. Error bars were drawn for two independent assays.

1

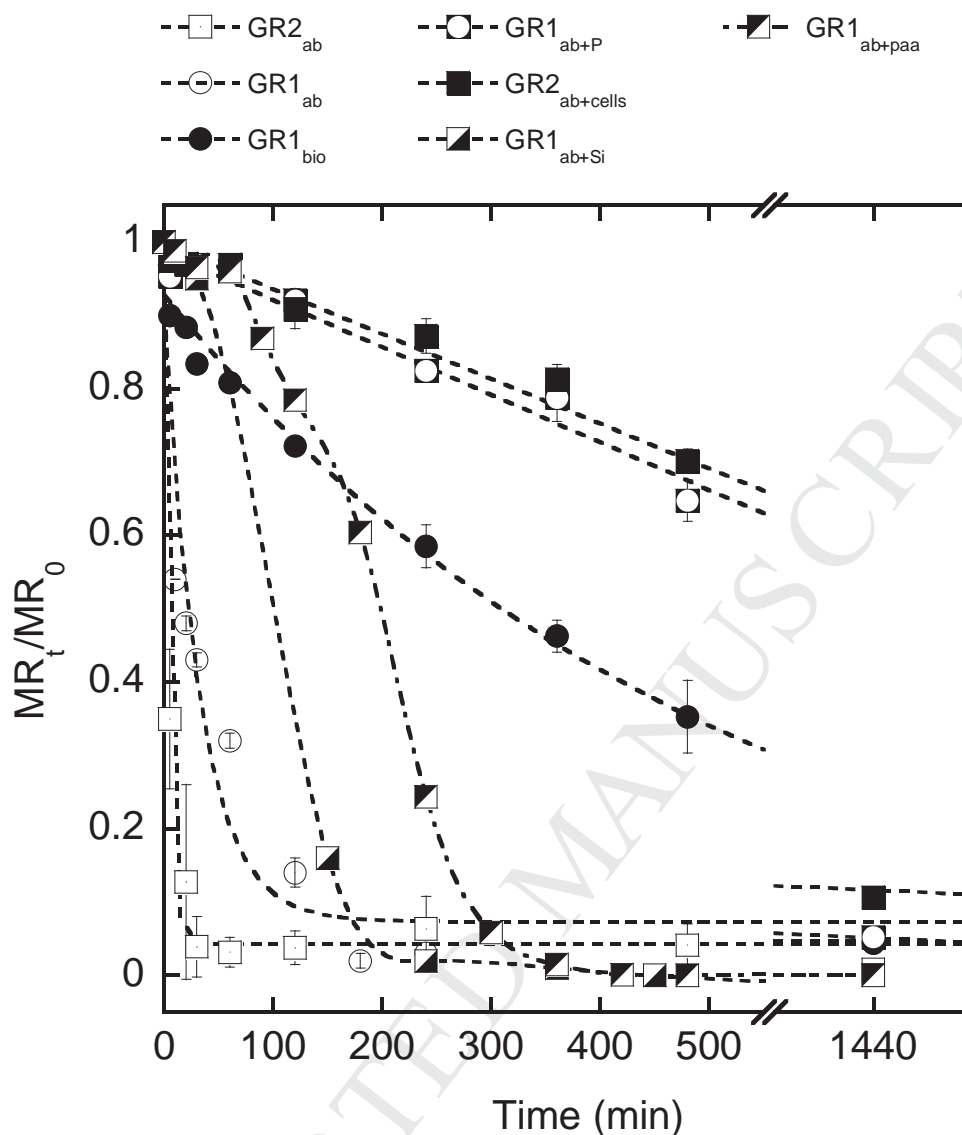


2

3

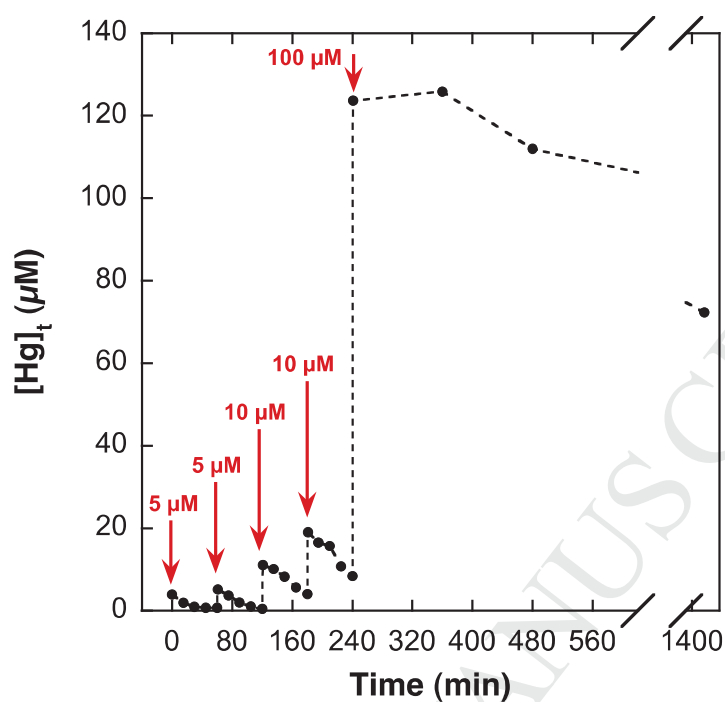
4 **Fig. 4.** – Green rust particles behavior at low/high pH and preferential adsorption/reduction of  
 5  $\text{Hg}(\text{OH})_2$ .

6



1  
2  
3 **Fig. 5.** Removal of methyl red (MR) in the presence of green rusts: 400  $\mu\text{M}$  of biologically  
4 synthesized hydroxycarbonate green rust ( $\text{GR1}_{\text{bio}}$ ), and 500  $\mu\text{M}$  of chemically synthesized  
5 hydroxycarbonate green rust ( $\text{GR1}_{\text{ab}}$ ),  $\text{GR1}_{\text{ab}}$  supplemented with phosphate ( $\text{GR1}_{\text{ab+P}}$ ), silicate  
6 ( $\text{GR1}_{\text{ab+Si}}$ ), polyacrylic acid ( $\text{GR1}_{\text{ab+paa}}$ ), hydroxysulfate green rust ( $\text{GR2}_{\text{ab}}$ ) and  $\text{GR2}_{\text{ab}}$   
7 supplemented with cells ( $\text{GR2}_{\text{ab+cells}}$ ). The MR remaining in solution ( $\text{MR}_t/\text{MR}_0$ ) is plotted as  
8 a function of time. The pH was manually held at a constant value of 7.0 before each sampling  
9 by addition of HCl 1M or NaOH 1M. Bars are the errors of two independent experiments.





1  
2  
3 **Fig. 6.** Kinetics of the Hg<sup>II</sup> reduction by biologically synthesized hydroxycarbonate green rust  
4 (GR1<sub>bio</sub>) with five successive additions of Hg<sup>II</sup> with an interval of one hour between each  
5 addition in the reaction medium containing an initial GR1<sub>bio</sub> concentration of 400 µM. The  
6 quantity of Hg<sup>II</sup> added each hour is indicated by the value above the red arrow. The total  
7 amount of Hg<sup>II</sup> added in the GR1<sub>bio</sub> suspension is 130 µM and after 24 h, 77 µM of Hg(II) was  
8 reduced into Hg<sup>0</sup>.

9  
10

1. The reactivity of green rusts (GR) towards  $\text{Hg}^{\text{II}}$  or methyl red (MR) was tested
2. Bacteria and phosphate did not affect GR reactivity with  $\text{Hg}^{\text{II}}$
3. Bacteria and ligands (phosphate, silicate and polymers) affect GR reactivity with MR
4. Environmental substances may hinder GR reactivity as regards to the target pollutant

1 Supplementary information of:

2

3 **Pseudo-first-order reaction of chemically and biologically formed green**  
4 **rusts with  $\text{Hg}^{\text{II}}$  and  $\text{C}_{15}\text{H}_{15}\text{N}_3\text{O}_2$ : effects of pH and stabilizing agents**  
5 **(phosphate, silicate, polyacrylic acid, and bacterial cells)**

6 P.-Ph. Remy<sup>1,2</sup>, M. Etique<sup>1,2</sup>, A.A. Hazotte<sup>1,2,§</sup>, A.-S. Sergent<sup>1,2</sup>, N. Estrade<sup>3,4#</sup>, C. Cloquet<sup>3,4</sup>,  
7 K. Hanna<sup>5,6</sup>, and F.P.A. Jorand<sup>1,2\*</sup>

8

9 <sup>1</sup>Université de Lorraine, LCPME, UMR 7564, Villers-lès-Nancy, F-54601, France

10 <sup>2</sup>CNRS, LCPME, UMR 7564, Villers-lès-Nancy, F-54601, France

11 <sup>3</sup>CNRS, CRPG, UMR 7358, BP 20, Vandœuvre-lès-Nancy, F-54501, France

12 <sup>4</sup>Université de Lorraine, CRPG, UMR 7358, BP 20, Vandœuvre-lès-Nancy, F-54501, France

13 <sup>5</sup>ENSCR, CNRS, UMR 6226, CS 50837, Rennes Cedex 7, F-35708, France

14 <sup>6</sup>Université européenne de Bretagne, Rennes, F-35000, France

15 <sup>§</sup>Present address: LUNAM University, Subatech-LPGN, UMR 6457 & 6112, BP 92208, F-  
16 44322 Nantes Cedex 3, France

17 <sup>#</sup>Present address: Pacific Centre for Isotopic and Geochemical Research, EOAS, The  
18 University of British Columbia, 2207 Main Mall, Vancouver, British Columbia, V6T 1Z4,  
19 Canada.

20

21 \*Corresponding author: frederic.jorand@univ-lorraine.fr; +33 (0)383 685 248

22

23 Table S1: Total mercury concentration in each compound used for experimentation with mercury test.

	<b>Pure water</b>	<b>SnCl<sub>2</sub></b>	<b>GR<sub>1</sub><sub>bio</sub></b>	<b>GR<sub>1</sub><sub>ab+P</sub></b>	<b>GR<sub>2</sub><sub>ab</sub></b>	<b>Sp</b>	<b>Fe<sup>II</sup><sub>aq.</sub></b>	<b>Hg<sup>II</sup></b>	<b>GR<sub>1</sub><sub>ab</sub></b>
<b>Hg (ppb)</b>	0.482	0.760	0.370	1.872	0.315	0.574	0.519	104.514	ND

24

25 Table S2a:  $d_{hkl}$  (nm) parameters from XRD analysis for chemically synthesized and biogenic carbonated green rust from the present study  
 26 (GR<sub>1</sub><sub>ab+P</sub>, GR<sub>1</sub><sub>ab</sub>, and GR<sub>1</sub><sub>bio</sub>) and from the literature <sup>a</sup>(Drissi *et al.*, 1995), <sup>b</sup>(Zegeye *et al.*, 2007).

27 n.d. : no data

Relative intensity	hkl	$d_{hkl}$	GR <sub>1</sub> <sub>ab+P</sub>	$d_{hkl}$	GR <sub>1</sub> <sub>ab</sub>	$d_{hkl}$	GR <sub>1</sub> <sub>bio</sub>	Ref <sup>a</sup> abiotic	Ref <sup>b</sup> biotic
100	003	0.759	0.758	0.759	0.758	0.759	0.751	0.751	0.751
32	006	0.377	0.379	0.377	0.379	0.378	0.373	0.373	0.375
1	101	0.274	-	0.274	-	0.274	0.273	0.273	n.d.
15	012	0.268	-	0.268	-	0.268	0.265	0.265	0.266
3	104	0.247	-	0.247	-	0.248	0.247	0.247	n.d.
12	015	0.235	0.235	0.235	0.235	0.235	0.233	0.233	0.233
1	107	0.209	-	0.209	-	0.209	0.208	0.208	n.d.
9	018	0.198	0.197	0.198	0.197	0.197	0.196	0.196	0.196
1	0012	0.189	0.189	0.189	0.189	0.188	0.188	0.188	n.d.
2	1010	0.175	-	0.175	-	0.174	0.173	0.173	n.d.

28

29

30

31 Table S2b:  $d_{hkl}$  (nm) parameters from XRD analysis for chemically synthesized hydroxysulfate green rust from the present study (GR2<sub>ab</sub>) and  
 32 from the literature <sup>a</sup>(Simon *et al.*, 1997), <sup>b</sup>(Hansen *et al.*, 1994).

33 n.d. : no data

34

Relative intensity	hkl	$d_{hkl}$ GR2 <sub>ab</sub>	Ref <sup>a</sup>	Ref <sup>b</sup>
100	001	1.091	1.09	1.10
80	002	0.547	0.545	0.549
60	003	0.365	0.362	0.366
20	004/100	0.276	0.275	0.275
30	101	0.67	0.266	0.226
30	102	0.246	0.245	n.d.
30	005/103	0.220	0.219	0.2195

35

36

37



51 Table S4. Values of pH for batch experiments (n=2)  
 52 before (initial pH) and after 60 min of incubation  
 53 (final pH) with Hg<sup>II</sup>.

Batch experiment	Initial pH	final pH
SnCl <sub>2</sub>	2.4	2.4
GR2 <sub>ab</sub>	7.0 ± 0.2	6.6 ± 0.1
	8.0 ± 0.1	7.2 ± 0.1
	9.5 ± 0.1	8.9 ± 0.3
GR2 <sub>ab+cells</sub>	7.0 ± 0.1	6.5 ± 0.1
GR1 <sub>bio</sub>	7.0 ± 0.1	7.2 ± 0.3
	8.1	8.0
	9.5 ± 0.1	9.0 ± 0.6
GR1 <sub>ab</sub>	8.2 ± 0.1	9.0 ± 0.1
GR1 <sub>ab+P</sub>	7.0 ± 0.1	7.6 ± 0.3
	8.0 ± 0.1	8.0 ± 0.2
	9.5 ± 0.1	8.8 ± 0.3
Fe <sup>II</sup> (2mM)	3.3 ± 0.1	3.5 ± 0.1

54

55

56 Note S1. Calculation of structural Fe<sup>II</sup>

$$57 \quad [\text{Fe}^{\text{total}}] = [\text{Fe}^{\text{II}}] + [\text{Fe}^{\text{III}}] = [\text{GR}] \times 6$$

$$58 \quad [\text{Fe}^{\text{II}}]/[\text{Fe}^{\text{III}}] = \text{Mössbauer ratio}$$

59 *e.g.* GR1<sub>ab+p</sub>

$$60 \quad [\text{Fe}^{\text{II}}] = 1.2 \times [\text{Fe}^{\text{III}}]$$

$$61 \quad 1.2 \times [\text{Fe}^{\text{III}}] + [\text{Fe}^{\text{III}}] = [\text{Fe}^{\text{total}}]$$

$$62 \quad [\text{Fe}^{\text{III}}] = [\text{Fe}^{\text{total}}]/2.2$$

$$63 \quad [\text{Fe}^{\text{II}}] = [\text{Fe}^{\text{total}}] - [\text{Fe}^{\text{total}}]/2.2 = 1.63 \text{ mM}$$

$$64 \quad [\text{Fe}^{\text{II}}]\text{GR1}_{\text{ab+p}} = 1.63 \times 10^{-3} \text{ M}$$

$$65 \quad [\text{Fe}^{\text{II}}]\text{GR1}_{\text{bio}} = 1.5 \times 10^{-3} \text{ M}$$

$$66 \quad [\text{Fe}^{\text{II}}]\text{GR2}_{\text{ab}} = 2 \times 10^{-3} \text{ M}$$

$$67 \quad [\text{Fe}^{\text{II}}]\text{GR1}_{\text{ab}} = 2 \times 10^{-3} \text{ M}$$

68

69 Note S2. Calculation of  $k_{\text{FeII}}$  ( $\text{L mol}^{-1} \text{ min}^{-1}$ ) =  $k_{\text{obs}}$  normalized to the structural Fe<sup>II</sup>  
70 concentration.

$$71 \quad k_{\text{FeII}} = k_{\text{obs}} / [\text{Fe}^{\text{II}}]\text{GR}$$

72 Where

73  $[\text{Fe}^{\text{II}}]\text{GR}$  is the structural Fe<sup>II</sup> concentration ( $\text{mol L}^{-1}$ )

74

75 Note S3. Calculation of  $k_s$  ( $\text{L mmol}^{-1} \text{ min}^{-1}$ ) =  $k_{\text{obs}}$  normalized to the surface Fe<sup>II</sup> sites ( $\mu\text{M}$ )  
76 (see manuscript)

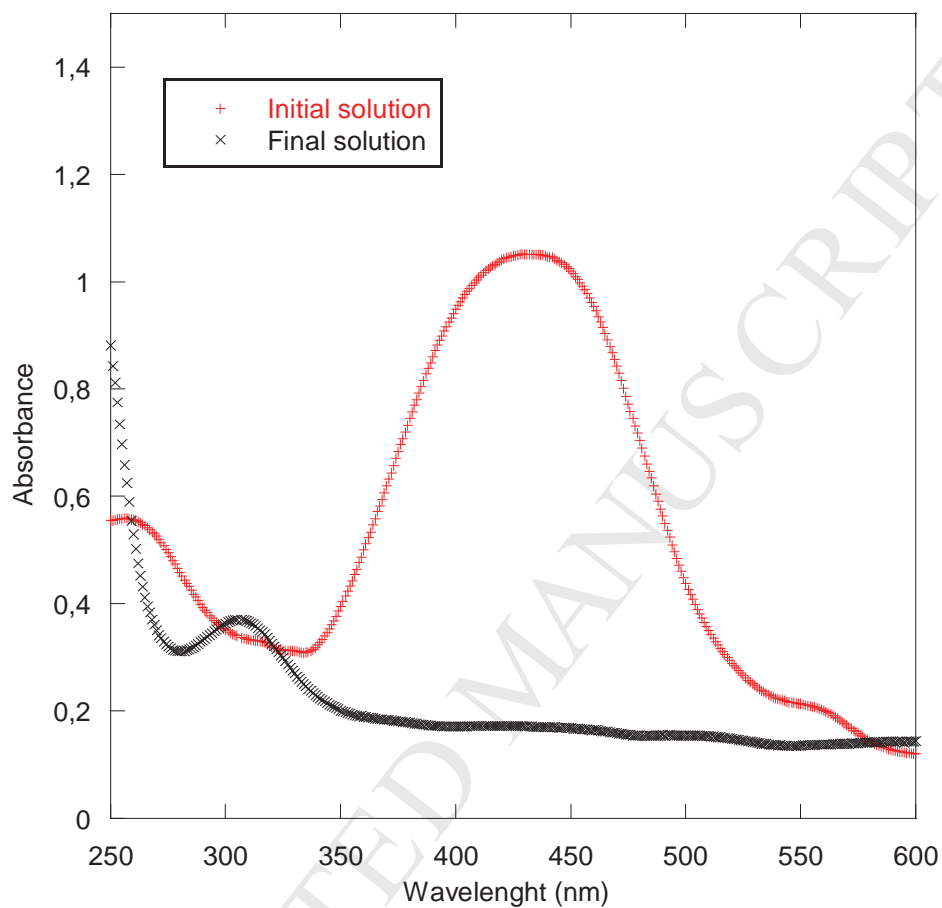
$$77 \quad k_s = k_{\text{obs}} / (\text{surface Fe}^{\text{II}} \text{ sites})$$

78

79

80

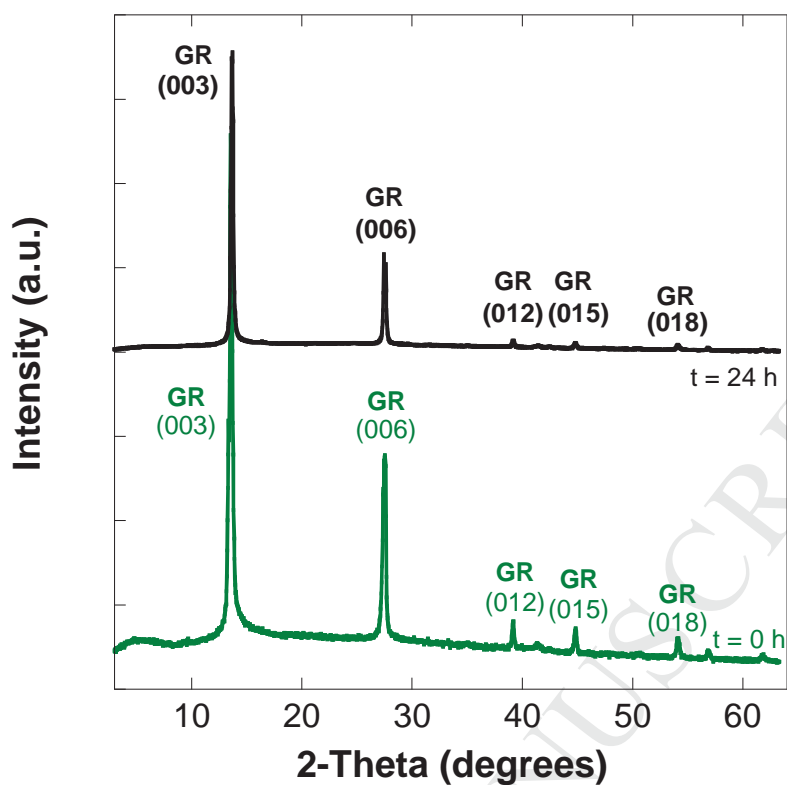




81

82 **Figure S1:** UV-Vis spectra of initial MR solution (+) and the same solution after 300 min of  
83 incubation with 500  $\mu\text{M}$  GR2<sub>ab</sub> (x).

84



85

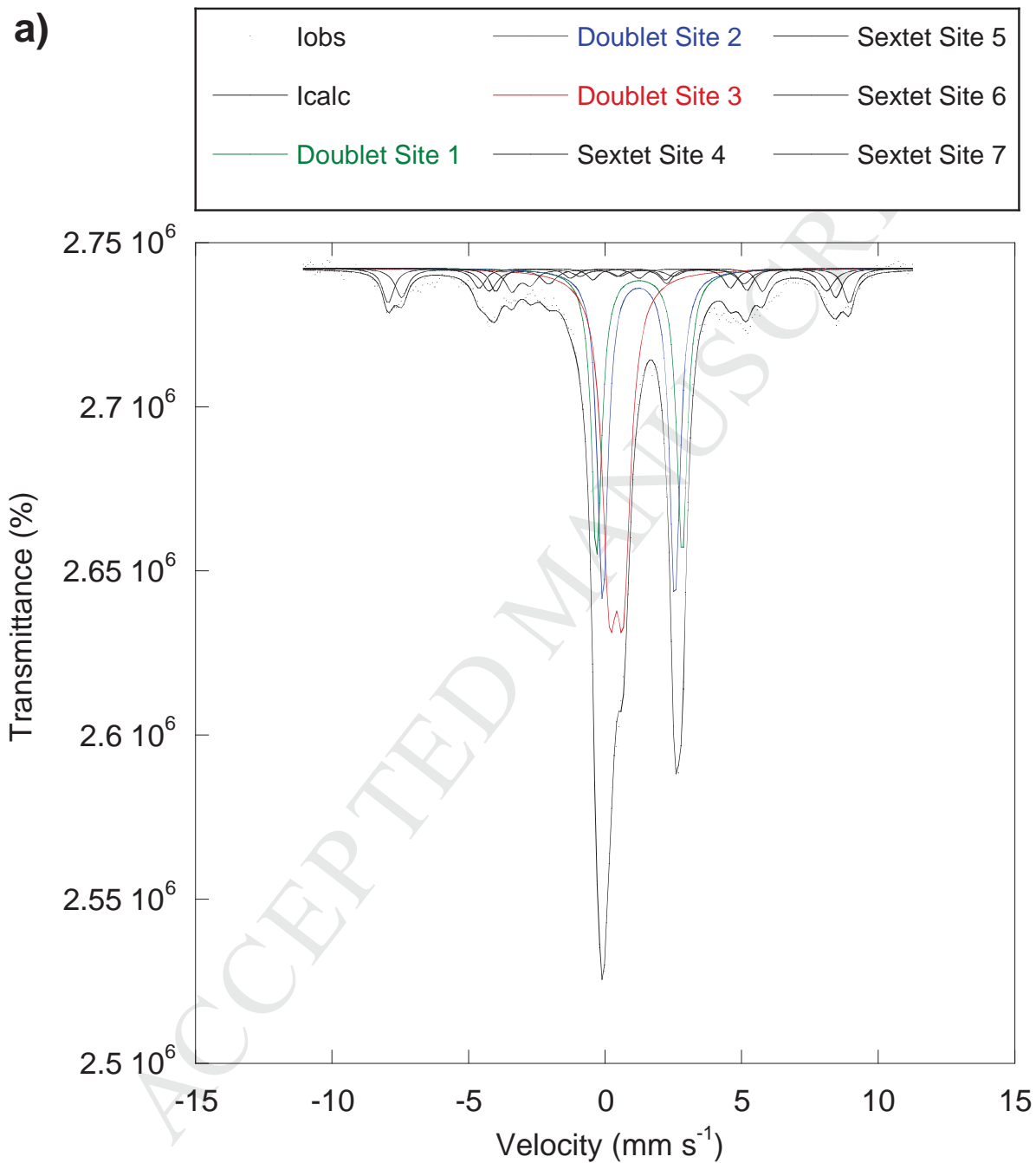
86 **Figure S2.** X-ray diffractograms of biologically synthesized hydroxycarbonate green rust  
87 (GR1<sub>bio</sub>) before addition of Hg<sup>II</sup> at the concentration of 5  $\mu$ M (green line, t = 0 h), and 24 h  
88 after (black line, t = 24 h). The initial concentration of GR1<sub>bio</sub> was 400  $\mu$ M. The lattice planes  
89 of green rust (GR) are written in brackets. The intensity is expressed in arbitrary unit (a. u.).

90

91

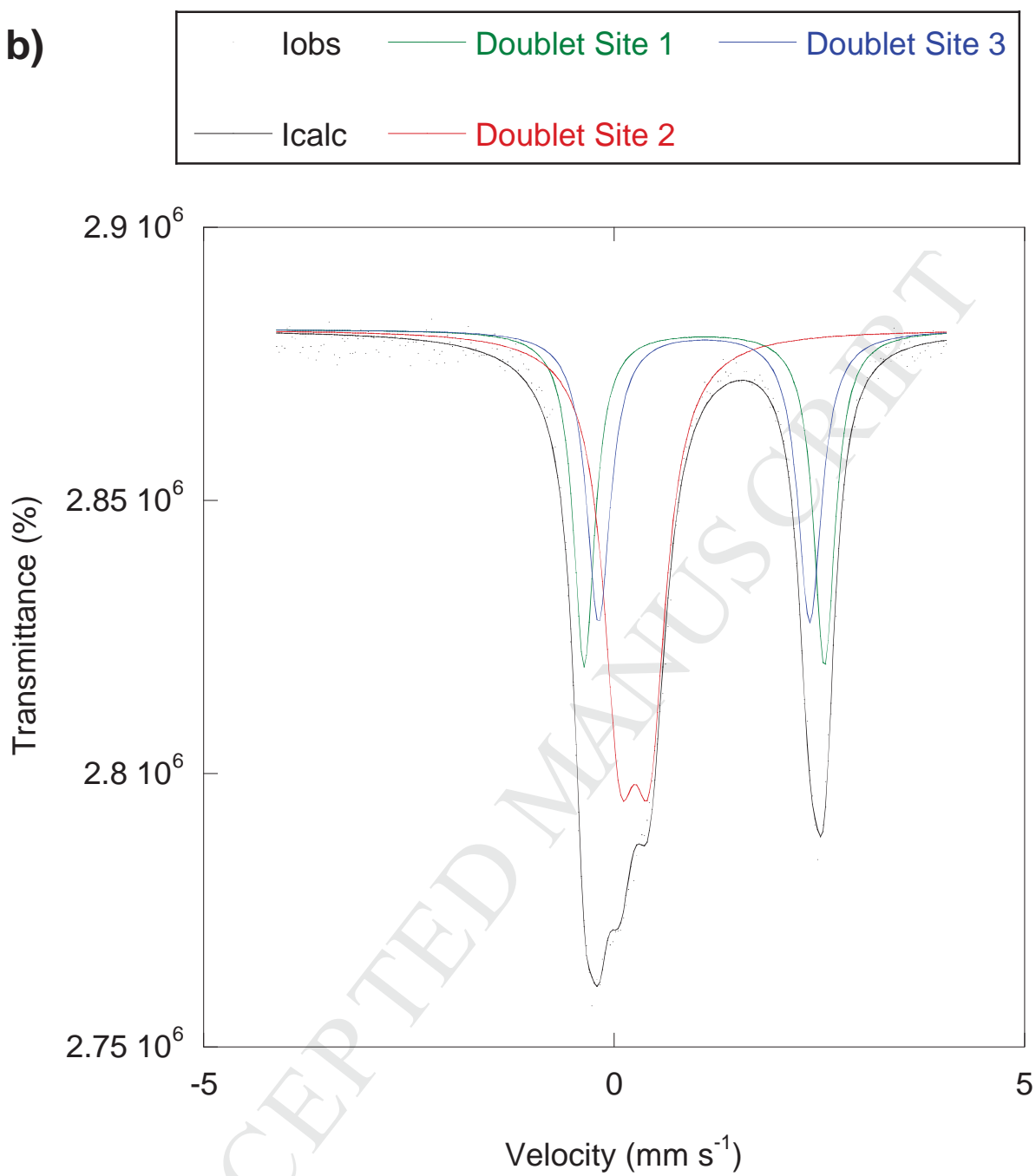
92 **Figure S3:** Mössbauer spectra of a) GR1<sub>bio</sub>, b) GR1<sub>ab+P</sub>, and c) GR2<sub>ab</sub>.

93



94

b)

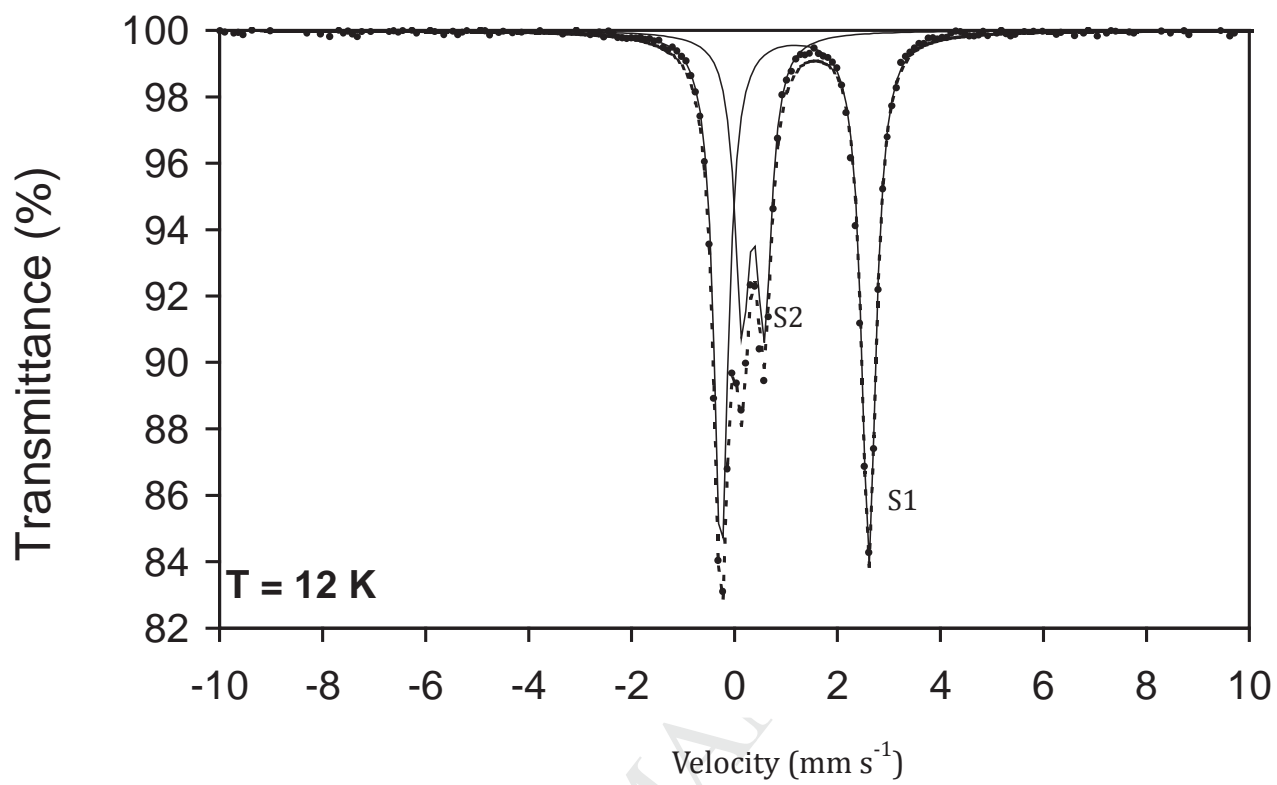


95

96 Fig. S3 b) GR1<sub>ab+P</sub>

97

98 c)

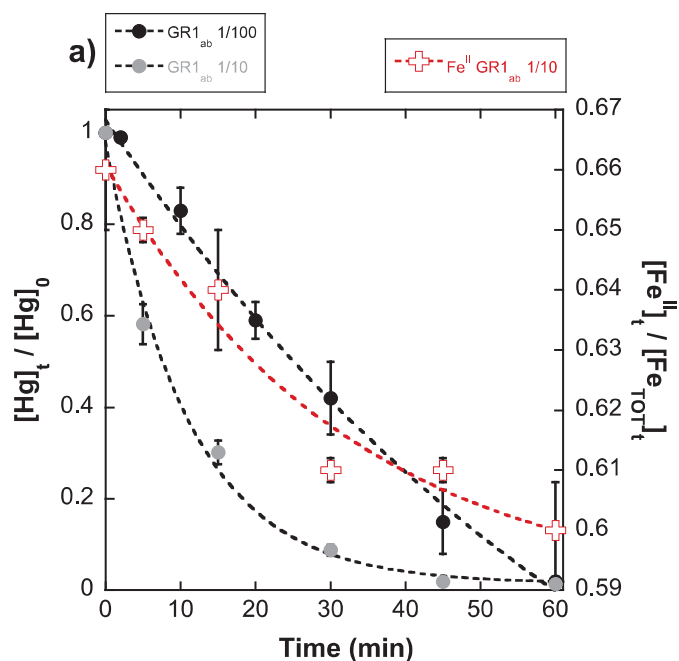


99

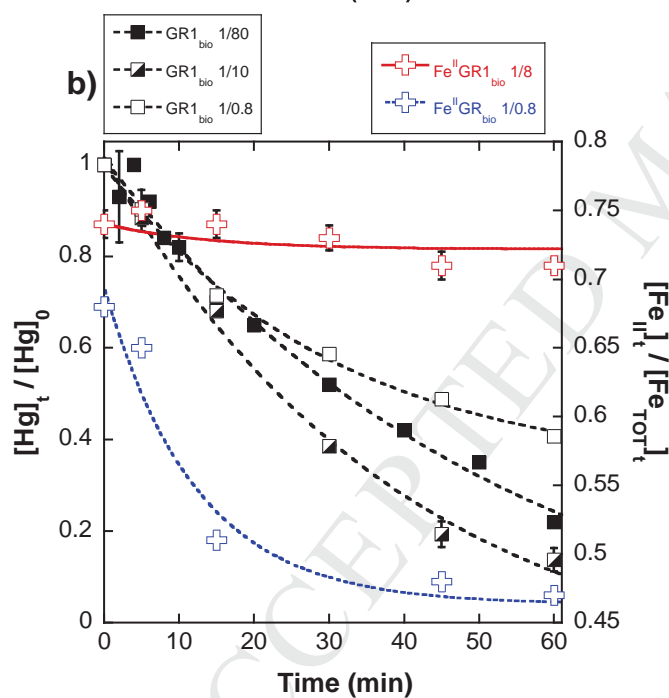
100 Figure S3c GR2<sub>ab</sub>

101

102



103

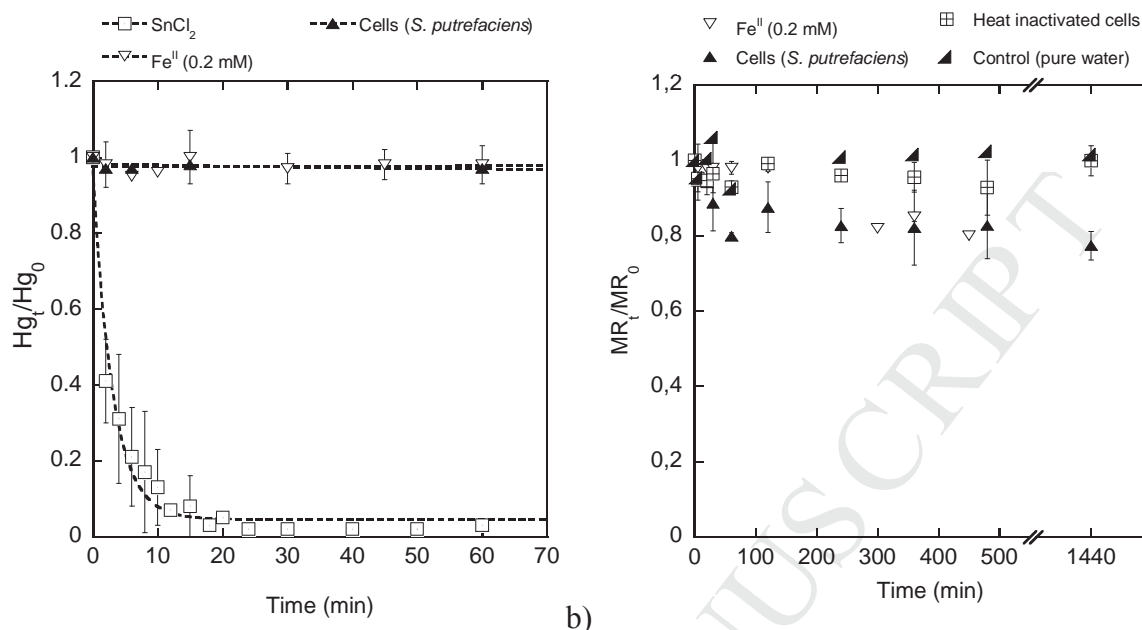


104

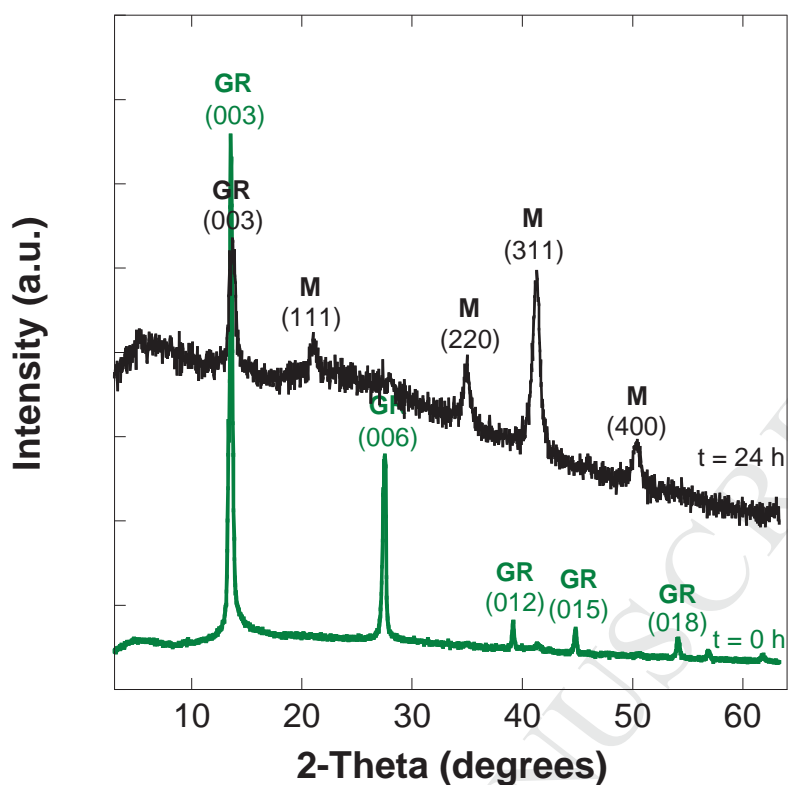
105 **Figure S4.** Removal of mercury and oxidation of ferrous iron content of chemically  
 106 synthesized green rust (GR1<sub>ab</sub>, a) and biologically formed green rust (GR1<sub>bio</sub>, b) over the time  
 107 at pH 8.2. The initial concentration of Hg<sup>II</sup> species was 5  $\mu\text{M}$  and the initial concentrations of  
 108 green rusts used were 4  $\mu\text{M}$ , 40  $\mu\text{M}$ , 400  $\mu\text{M}$  for GR1<sub>bio</sub>, and 50  $\mu\text{M}$ , 500  $\mu\text{M}$  for GR1<sub>ab</sub>. The  
 109 Hg<sup>II</sup>/GR ratios were 1/0.8, 1/8, 1/80 and 1/10, 1/100 respectively. Error bars were drawn for  
 110 two independent assays.

111

112



113 a) 114 **Figure S5.** (a): Disappearance of mercury over time in the presence of 50  $\mu M$   $Sn^{II}$  (pH  
115  $3.0 \pm 0.5$ ), and 0.2 mM aqueous  $Fe^{II}$  (pH  $7.0 \pm 0.1$ ) or  $6 \times 10^5$  cells  $mL^{-1}$  of *Shewanella*  
116 *putrefaciens* (pH  $7.0 \pm 0.1$ ) (cells), a cell density that is equivalent to that used for the  
117 synthesis of  $GR_{bio}$  and that is expected to remain with  $GR1_{bio}$ . The changes in pH after a 60 h  
118 incubation time period are reported in Table S7. Bars are the errors of two independent  
119 experiments. The stannic solution ( $SnCl_2$ , 50  $\mu M$  pH = 3) was prepared from a stock solution  
120 (22.5 mM in HCl 1.5 M) ( $SnCl_2$  salt, 98% anhydrous, 196981000, Acros). It was used as an  
121 indicator for  $Hg^{II}$  reduction, since  $Sn^{II}$  is known to be a powerful reducer (Zheng and  
122 Hintelmann, 2010). In order to avoid  $Sn^{II}$  precipitation, which can occur along with increasing  
123 pH,  $Hg^{II}$  reduction by aqueous  $Sn^{II}$  were only performed at pH 3.  
124 (b): Disappearance of methyl red (MR) over time in the presence of 0.2 mM aqueous  $Fe^{II}$  (pH  
125 7.0),  $6 \times 10^5$  cells  $mL^{-1}$  of a fresh *S. putrefaciens* suspension (cells) or heat inactivated cells  
126 (dead Sp cells), or a solution of MR in pure water.  
127



128

129 **Figure S6.** X-ray diffractograms of biologically synthesized hydroxycarbonate green rust  
130 (GR1<sub>bio</sub>) before addition of Hg<sup>II</sup> at the concentration of 5  $\mu$ M (green line,  $t = 0$  h), and 24 h  
131 after (black line,  $t = 24$  h). The initial concentration of GR1<sub>bio</sub> was 4  $\mu$ M. The green rust (GR)  
132 was oxidized into magnetite (M) during the reduction of mercury. The lattice planes are  
133 written in brackets. The intensity is expressed in arbitrary unit (a. u.).

134



135

136 References for supplementary data:

- 137 Bocher, F., Géhin, A., Ruby, C., Ghanbaja, J., Abdelmoula, M., Génin J.-M.R. 2004.  
138 Coprecipitation of Fe(II–III) hydroxycarbonate green rust stabilized by phosphate  
139 adsorption. *Solid State Sciences*, 6 (1), 117–124.
- 140 Drissi, SH, Refait, P, Abdelmoula, M, Génin, J.-M.R. 1995. The preparation and  
141 thermodynamic properties of iron(II)-iron(III) hydroxide-carbonate (green rust); Pourbaix  
142 diagram of iron in carbonate-containing aqueous media. *Corrosion Science* 37, 2025–  
143 2041.
- 144 Hansen H. C. B., Borggaard O. K., Sorensen J. 1994. Evaluation of the free energy of  
145 formation of Fe(II)-Fe(III) hydroxide-sulphate (green rust) and its reduction of nitrite.  
146 *Geochimica et Cosmochimica Acta* 58, 2599-2068.
- 147 Ruby, C., Haissa, R., Géhin, A., Abdelmoula, M., Génin, J.-M.R., 2006. Chemical stability of  
148 hydroxysulphate green rust synthesized in the presence of foreign anions: carbonate,  
149 phosphate and silicate. *Hyperfine Interactions*, 167: 803-807.
- 150 Simon L., Francois M., Refait P., Renaudin G., Lelaurain M., and Génin J.-M. R., 2003.  
151 Structure of the Fe(II-III) layered double hydroxysulphate green rust two from Rietveld  
152 analysis. *Solid State Sciences* 5, 327–334.
- 153 Zegeye, A., Ruby, C., Jorand, F., 2007. Kinetic and thermodynamic analysis during  
154 dissimilatory  $\gamma$ -FeOOH reduction: formation of green rust 1 and magnetite.  
155 *Geomicrobiology Journal* 24, 51-64.
- 156 Zheng, W., Hintelmann, H., 2010. Nuclear field shift effect in isotope fractionation of  
157 mercury during abiotic reduction in the absence of light. *The Journal of Physical*  
158 *Chemistry A* 114 (12), 4238-4245.